

**THEORY FOR THE EFFECT OF POLYDISPERSITY
ON THE PHASE BEHAVIOUR OF DIBLOCK
COPOLYMERS**

By

DAVID M. COOKE, B.Sc.

A Thesis
Submitted to the School of Graduate Studies
in Partial Fulfillment of the Requirements
for the Degree
Master of Science

McMaster University
©Copyright by David M. Cooke, 2002.

MASTER OF SCIENCE (2002)
(Physics)

McMaster University
Hamilton, Ontario

TITLE: Theory for the effect of polydispersity on the phase behaviour of diblock copolymers

AUTHOR: David M. Cooke, B.Sc.(SFU)

SUPERVISOR: Dr. A.-C. Shi

NUMBER OF PAGES: vii, 67

To my mother, who understands.

Acknowledgements

I couldn't have done this without the loving support of my parents, and their continual worrying about their son. I'd also like to thank my sisters, Jen and Amy, for not complaining too loudly about missed birthday presents.

I'd like to thank my officemate Pat Byrne for his hard-working example, and the members of our group, Rob Wickham, Karim Jaffer, and Josie Lee, for their advice and explanations. Also, thanks to Bill Coish, Soko Matsumura, Jamal Sakhr, and Dan Knapp, for being in late at night and listening to my rantings.

My supervisor, An-Chang Shi, deserves much credit for seeing me through this, even as it stretched on and on. I'm also indebted to my committee, John Berlinsky and Kari Dalnoki-Veress, for their patience as I stumbled.

I'd especially like to thank my cat, Gus, for listening.



Abstract

Polymers are one of the most prevalent types of molecules in modern life. These long macromolecules make up everything from DNA to plastics to Jell-O™. An interesting class of polymers are block copolymers, which are composed of two (or more) chains, or blocks, of chemically distinct monomers covalently bonded end-to-end to form a single polymer. Different types of polymers tend to avoid each other, but since block copolymers are joined together the polymer species can not macroscopically phase separate. Instead, they separate on the scale of the size of the polymers, forming nanostructures. For a diblock copolymer melt, which is made from two types of polymers, these nanostructures can be, depending on the ratio of the length of one block to the other, spheres, cylinders, lamellae, or the more bizarre gyroid phase.

Self-consistent field theory (SCFT) as formulated by Helfand in 1975 has in recent years been successfully applied to the study of the phase behaviour of diblock copolymers. However, most of the studies assume that the polymers are monodisperse, while almost all polymer melts are polydisperse. This work examines the effect of polydispersity in the block lengths on phase behaviour of diblock copolymer melts, by developing the SCFT for polydisperse block copolymers. The theory is examined using a perturbation method, as well as the random-phase approximation (RPA). The perturbation parameter is the ratio κ of the weight-averaged molecular weight and the number-averaged molecular weight, which is a common measure of polydispersity.

The results show polydispersity shifts the transition from a disordered phase to an ordered phase to a higher temperature, and increases the period of the nanostructures. It is also observed that polydispersity leads to larger non-lamellar phase regions in the phase diagrams. Results from the RPA also suggest that macrophase separation occurs for large polydispersities.

Table of Contents

1	Introduction	1
2	Self-Consistent Field Theory	10
2.1	Overview of polydisperse polymer melts	10
2.2	Self-consistent field theory	12
3	Random Phase Approximation	24
4	Implementation	33
4.1	Perturbative polydispersity	38
5	Results and Discussion	40
5.1	Phase diagrams	43
5.2	Periodicity	47
5.3	Scaling	52
6	Summary	54
A	The Gamma Symbol	56
A.1	Structure of a space group	57
A.2	Basis functions	59
A.3	Simplification of Γ_{nml}	63
	Bibliography	63

List of Figures

1.1	Phase diagram for a monodisperse diblock copolymer melt.	4
1.2	Pictures of the phases at $\chi N = 12$ for monodisperse melt.	5
1.3	A schematic GPC plot.	7
2.1	Schultz-Zimm distribution for various values of k	13
3.1	Structure factor for the monodisperse case, and for the polydisperse distributions at $f = 0.5$, $\chi N = 8$	29
3.2	Scaled incompressibility-corrected structure factor	30
3.3	Dependence of the position of the critical point on the polydispersity.	32
5.1	Free energy of the hex and gyroid phases.	42
5.2	Comparison of the ODT as found with SCFT to the spinodal line calculated using the RPA for $f = 0.48$	44
5.3	Phase diagrams for diblock melts where each block is equally polydisperse.	45
5.4	Phase diagrams for diblock melts with one block monodisperse.	46
5.5	Change in period as κ increases for the four phases	48
5.6	Change in period for the lamellar phase at $f = 0.5$	49
5.7	The decile composition of the hex phase at $\chi N = 13.5$, $f = 0.35$, $\kappa = 0.2$	50
5.8	Illustration of monodisperse vs. polydisperse polymer packing	51
5.9	Scaled phase diagrams for the symmetric polydisperse melts	52

Chapter 1

Introduction

Reeling and Writhing, of course, to begin with, the Mock Turtle replied, and the different branches of Arithmetic – Ambition, Distraction, Uglification, and Derision.

Lewis Carroll, Alice in Wonderland. Chap. x.

Mixtures of different polymers tend to phase separate at some range of temperatures due to incompatibility between different types of monomers. Mixtures of homopolymers tend to separate on a macroscopic scale in accordance with the “lever rule” for minimising the free energy [Doi97, page 26]. Block copolymers, formed of covalently bonded polymer chains, can not separate different monomer types by distances greater than the size of the polymer, so macroscopic separation of the different monomers is impossible. Instead, they will form domains whose size is on the order of the length of the polymer. This leads to nanoscopic structures of various symmetries [Lei80, MB96, HSK80, HS82].

A diblock copolymer is a linear polymer made of two polymer blocks, A and B, joined end-to-end by a covalent bond. The phase diagram for a diblock copolymer melt was first constructed by Leibler in 1980 using an expansion of the free energy in powers of the monomer density [Lei80]. It predicted the existence of lamellar, cylindrical (arranged in a hexagonal structure), and spherical (arranged in a

body-centered cubic structure) phases. However, this mean-field theory was only accurate in the so-called weak-segregation limit (WSL), in which the spatial variation of the densities is assumed to be very small. In 1975, Helfand had developed the self-consistent field theory (SCFT) which applies to all degrees of segregation; unfortunately, it requires more computing resources than Leibler's theory [Hel75]. Approximate numeric solutions of SCFT were obtained by, Helfand and, among others, Whitmore and coworkers [Hel75, WN90, WV92]. SCFT didn't come into its own until 1994 when Matsen and Schick used a reciprocal space expansion, along with cheap computing power that Helfand didn't have, to predict the full phase diagram [MS94]. It is this theory and technique which will be used in the present work.

As mentioned above, two theories used for examining the phase diagrams of block copolymer melts are Leibler-like theories, and self-consistent field theories. These are both mean-field theories; the interactions between the polymers are assumed to be mediated by a coarse-grained field. There is one other type of theory that has enjoyed some success: the strong-segregation limit by Semenov, where the interfaces between different monomer types are assumed to be sharp [Sem85]. This limit is valid for low temperatures. Leibler theories are, in general, valid only for high temperatures near the order-disorder transition, but self-consistent theories are valid for weak and intermediate segregations.

As an extension of the mean-field theories, the random phase approximation (RPA) has been used with reasonable success to predict the structure factor for the non-phase separated (homogeneous) state of a blend of block copolymers [HN84, BRS90]. By using the exact mean-field solution, Gaussian fluctuations can be included to determine the density-density correlation functions, which in turn gives the structure factors. Using the RPA Hong and Noolandi examined the structure factors for polydisperse diblock copolymer in 1984 [HN84].

Each block of a diblock copolymer has a degree of polymerization (number of

repeat units in the molecule) N_A and N_B . The total length of the chain is $N = N_A + N_B$. The fraction of block A in the polymer is $f_A = N_A/N$. The interaction between different monomer types is characterised by the parameter $\chi = a + b/T$, where T is the temperature and a and b are phenomenological constants. The phase diagram of a monodisperse diblock copolymer melt calculated from self-consistent field theory (as described in Chapter 2) is given in Figure 1.1. The results from SCFT turn out to depend on the interaction parameter and the degree of polymerization through the combined parameter χN . The phase diagram is symmetric and all transition lines are roughly parabolas. There are five phases in the diagram: a homogeneous phase at high temperatures (low χ), and four ordered phases, whose structures are illustrated in Figure 1.2. Proceeding from the homogeneous region through the order-disorder transition (ODT), the system orders into spherical micelles arranged on a three-dimensional bcc structure. The minority component of the diblocks form the inside of spheres which are embedded in a bulk matrix of the majority component. As χN is increased, the melt forms cylinders arranged on a hexagonal lattice; a two-dimensional structure. For symmetric diblocks, a one-dimensional lamellar phase is formed for still higher χN . However, for sufficiently asymmetric diblocks, a three dimensional double gyroid phase (space group $Ia\bar{3}d$, #230 in the International Tables for Crystallography [Hah99]) is found. This structure is composed of two interpenetrating sub-lattices with a connectivity of three. One of the successes of SCFT over the strong-segregation limit (SSL) theory [Sem85] and the weak-segregation limit theory [Lei80] has been its prediction of the gyroid phase. There is a triple point between the hex, gyroid, and lamellar phases at $f_t = 0.45$ and $\chi N_t = 11.16$. The critical point at $f_c = 0.5$ and $\chi N_c = 10.495$ is a second-order phase transition within the mean-field approximation. However, including fluctuations in SCFT renders it weakly first-order [FH87, Bra75].

While three of the phases, one-dimensional lamellae, two-dimensional cylinders, and three-dimensional spheres, could have been expected on simple physical

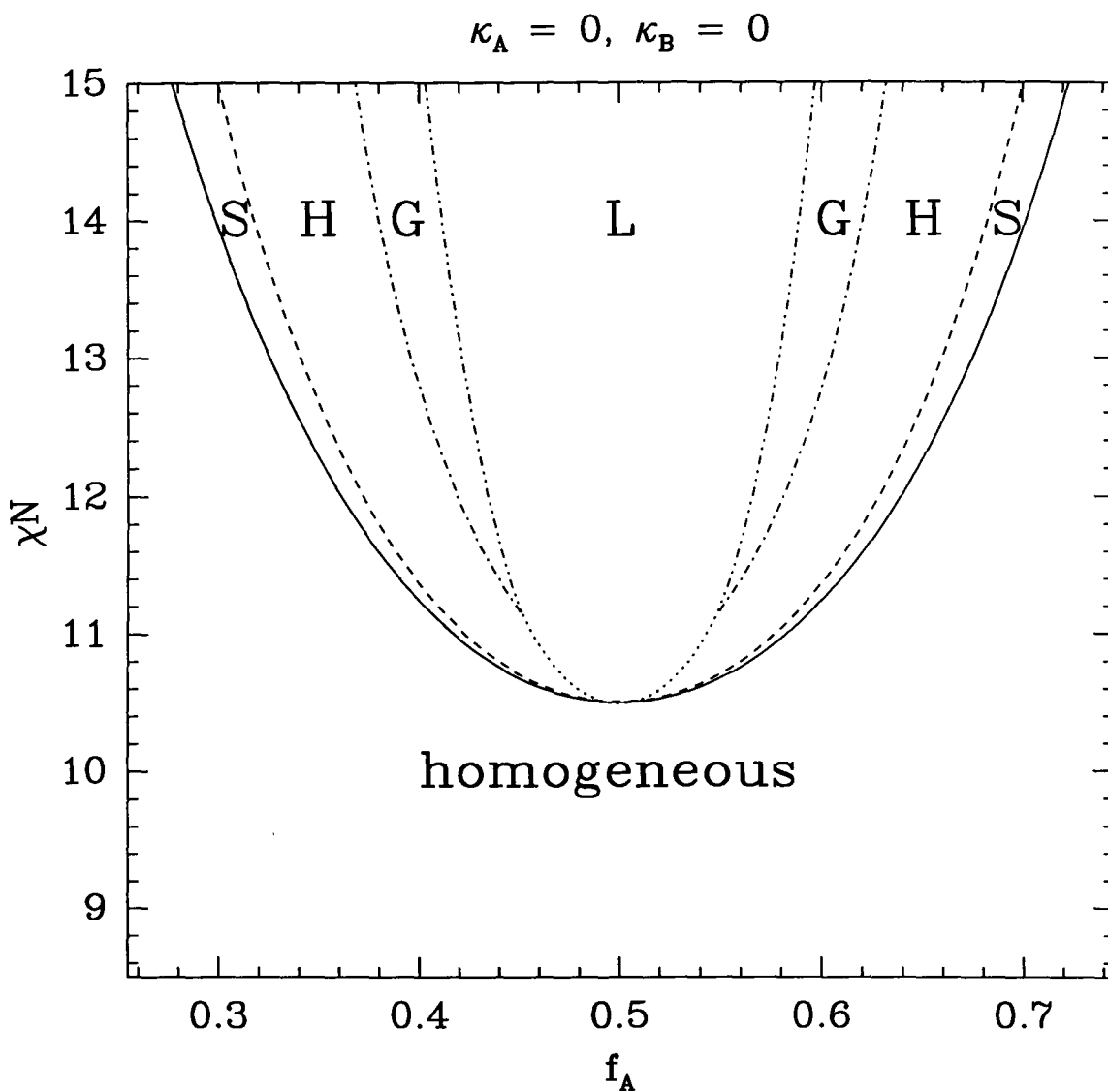


Figure 1.1: Phase diagram for a monodisperse diblock copolymer melt. From inside out, the phases are: *L* – lamellar, *G* – double gyroid, *H* – hexagonal cylindrical, and *S* – bcc spherical micelles. Outside of the microstructure phases is a disordered phase.

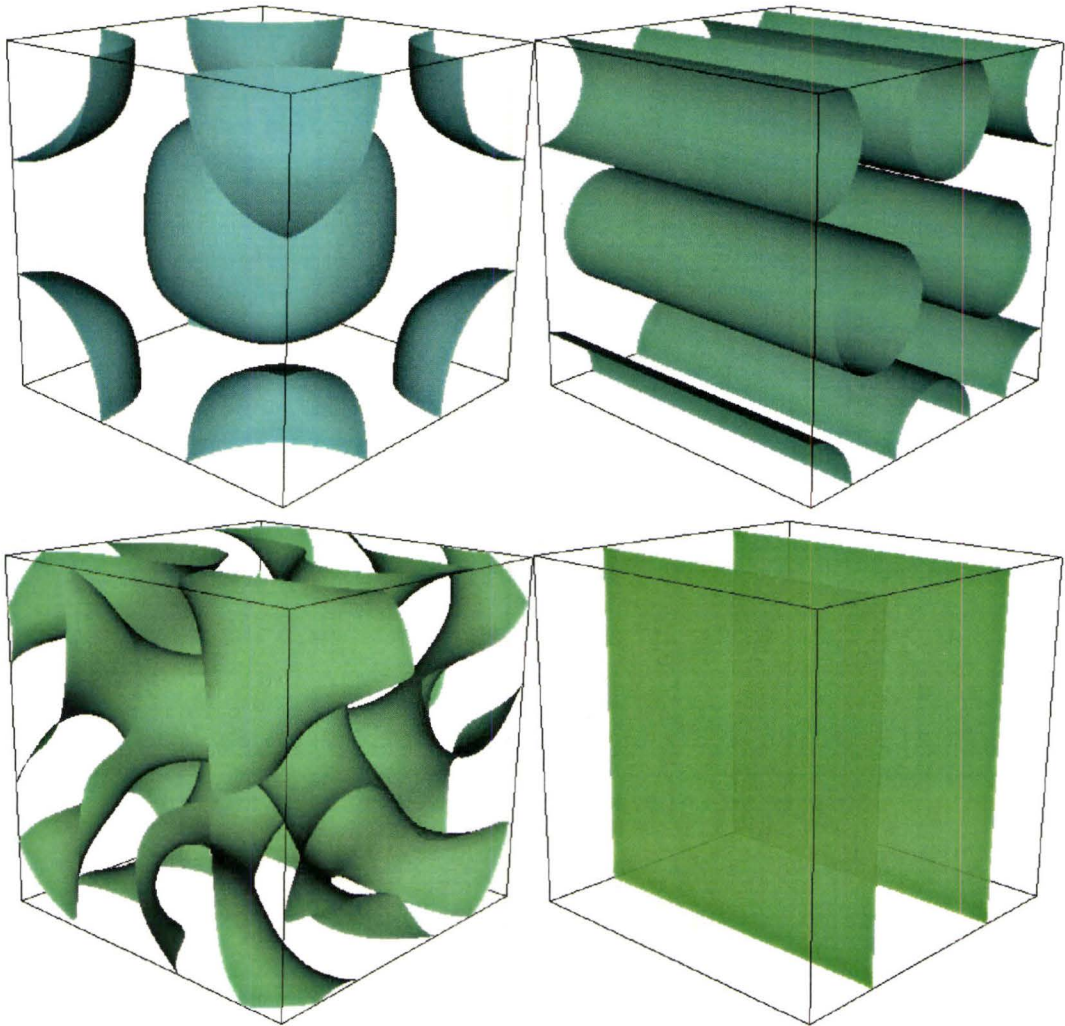


Figure 1.2: Pictures of the phases at $\chi N = 12$. Clockwise from top left: bcc at $f = 0.38$, hex at $f = 0.4$, lamellar at $f = 0.5$, and gyroid at $f = 0.42$. These are isosurfaces of the density profile where the density equals the average volume fraction. Note that these are not to scale: the gyroid should be about twice the size of the lamellar period.

grounds the double gyroid phase is a surprise. Early on in the study of diblock copolymer melts, the gyroid phase was indentified with a double-diamond phase (Hermann-Mauguin symbol $Pn\bar{3}m$, #229, with a connectivity of four). This was mainly due to the fact that the two phases have similiar reciprocal lattice spaces. Experimentally, another phase, a hexagonally-perforated lamellar phase is often observed, but this is judged to be a metastable phase [MB96]. Since the timescale for relaxation of polymers can be very long (on the order of years or decades [Str97]), it is difficult to determine whether a phase is stable or “merely” metastable.

Most theories of polymer phase separation assume that polymers of the same type are monodisperse (all the same length); however, this is difficult or impossible to realize in the lab, let alone in industrial processes. Monodisperse polymer systems are more tractable theoretically than polydisperse ones, if only for the fewer system parameters to be specified. However, in the real world, polydispersity can not be avoided; it is intrinsic to the methods used to make polymers. Polydisperse polymers are the norm, not the exception, and understanding how polydispersity changes the predictions of monodisperse theories is important.

The distribution of molecular weights in a sample of a polymeric material comes from the inherent random nature of the growth of the polymers. Chain growth occurs because of the random encounters between reactive species. There is no process (besides biological ones for making proteins and other biomolecules) that will stop chain growth at an *a priori* specified length. Instead, termination will occur when the concentration of reactive species is too low (as in condensation polymerization), or when a terminating molecule reacts with the growing end.

The distribution of chain lengths is measurable with a size-exclusion chromatography (SEC) technique such as gel permeation chromatography (GPC), which give the fraction of molecules with a given molecular weight [Kro90]. A schematic GPC graph is given in Figure 1.3. While the full distribution of chain lengths is useful, most such distributions are usefully characterised by two parameters: the number

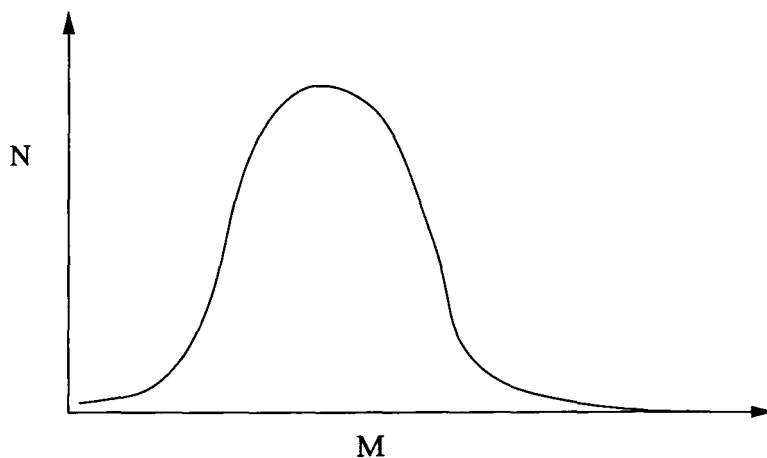


Figure 1.3: A schematic GPC plot.

average molecular weight \bar{M}_n and the polydispersity index \bar{M}_w/\bar{M}_n , where \bar{M}_w is the weight average molecular weight.

\bar{M}_n and \bar{M}_w are defined as follows. Let the total number of molecules be n_t , and divide the molecules into classes such that there are n_i molecules in the i th class each with a mass of M_i . Also, let $f_i = n_i/n_t$ be the fraction of molecules in the i th class. Then the two averages of interest are

$$\bar{M}_n = \sum_i f_i M_i = \langle M \rangle \quad (1.1)$$

$$\bar{M}_w = \frac{\sum_i f_i M_i^2}{\sum_i f_i M_i} = \frac{\langle M^2 \rangle}{\langle M \rangle} \quad (1.2)$$

The measure of the polydispersity $\kappa \equiv \bar{M}_w/\bar{M}_n - 1$ is then

$$\kappa = \frac{\langle M^2 \rangle - \langle M \rangle^2}{\langle M \rangle^2}. \quad (1.3)$$

It is easy to show that

$$\kappa = \frac{\sigma^2}{\overline{M}_n^2} \quad (1.4)$$

where σ is the standard deviation of the chain length distribution. Thus, κ is a measure of the width of the distribution. Also, note that $\kappa > 0$ always (and hence $\overline{M}_n/\overline{M}_w > 1$). In the literature, since true monodisperse polymers are rare, “monodisperse” tends to refer to polymers with narrow polydispersity distributions from $\kappa \approx 0.03$ to at most about 0.3, and “polydisperse” refers to broader distributions, with $\kappa \gtrsim 0.5$.

The chain distribution depends on polymerization processes. Polymerization techniques can be broadly grouped into two classes: *step-growth*, and *chain-growth* polymerization [Hie84]. Step-growth polymerization, or condensation, proceeds in a step-wise fashion. The reacting species are polymer molecules AB. Each individual reaction step is an reaction between two such molecules, occurring between the reactive ends A and B, forming a larger molecule AabB. Chain-growth polymerization, however, proceeds by a chain reaction. Starting with an initiation species I, a functional group adds itself on to the end of a growing (“live”) polymer, as in $IM_n^* + M \rightarrow IM_{n+1}^*$, until the growing end is terminated by some means, or the monomers are exhausted.

It can be shown that for step-growth polymerization, as the reaction proceeds to completion, the polydispersity of the resulting polymer melt goes to $\kappa = 1$ [Hie84]. This type of polymerization is used to make such common polymers as poly(ethylene terephthalate) (Dacron or Mylar), poly(hexamethylene adipamide) (nylon), and poly(tetramethylene hexamethylene urethane) (spandex) [Hie84].

Chain-growth, or addition, polymerization, is used for such polymers as polyethylene, polystyrene (Styrofoam), poly(vinyl chloride) (PVC or vinyl), polyacrylonitrile (acrylic), poly(methyl methacrylate) (PMMA or Plexiglas), and polytetrafluoroethylene (Teflon). Most of the block copolymers studied experimentally are

made by chain-growth polymerization.

In this work, the effect of polydispersity on the phase behaviour of a diblock copolymer melt is studied. The approach taken here is to use SCFT, and to characterise the polydispersity by the moments of the molecular weight distribution expanded about its average. The theoretic framework for polydisperse diblock copolymer systems is developed, along with a method for solving the mean-field equations numerically. The results obtained from this can be compared to the results from a random-phase approximation in the homogeneous phase.

Chapter 2

Self-Consistent Field Theory

We can lick gravity, but sometimes the paperwork is overwhelming.

Wernher von Braun

2.1 Overview of polydisperse polymer melts

A blend of polymers is made up of different molecular species, which have different attributes such as chain length and chemical composition. A polydisperse polymer melt can be viewed as a polymer blend composed of monodisperse polymers with different molecular weights. For each polymer, an index σ can be attached. The distribution of polymers can then be described by a probability distribution $P(\sigma)$, so in a volume V , there are

$$n_\sigma = n_c P(\sigma) \tag{2.1}$$

polymer molecules with the index σ , where the total number of polymers is n_c . The index σ can contain information about the chemical composition, charge, and degree of polymerization. Polydispersity in the chemical composition for a random copolymer has been considered previously by Angerman *et. al.* [Ang98, AtBS99]. Here, a diblock copolymer melt will be considered. The polydispersity will be in

the degrees of polymerization of each of the two blocks making up the polymer molecules. The index is then two numbers, representing the degree of polymerization of the two blocks. Letting the average polymerization of the A and B blocks be \bar{N}_A and \bar{N}_B , respectively, the polymerization indices will be taken as $\sigma_\alpha = N_\alpha/\bar{N}_\alpha$, where N_α is the polymerization of the α block of the specific polymer molecule in question (the Greek letters α and β will be used to denote monomer types from now on). By definition, the average of σ_α is 1. The polymerizations of the two blocks will also be assumed to be independent, so that the polymer distribution $P(\sigma) = P(\sigma_A, \sigma_B)$ can be factored as $P(\sigma_A, \sigma_B) = P_A(\sigma_A)P_B(\sigma_B)$. By definition, then,

$$\bar{N}_\alpha = \int_0^\infty d\sigma_\alpha P_\alpha(\sigma_\alpha) \bar{N}_\alpha \sigma_\alpha. \quad (2.2)$$

For convenience (since the index σ is two numbers $(\sigma_\alpha, \sigma_\beta)$), $N_\alpha(\sigma)$ will be defined as $\bar{N}_\alpha \sigma_\alpha$. Also, $N(\sigma) = N_A + N_B$. The average $\langle f \rangle_\sigma$ of a quantity $f(\sigma_A, \sigma_B)$ is defined as

$$\langle f \rangle_\sigma = \int_0^\infty \int_0^\infty d\sigma_A d\sigma_B P_A(\sigma_A) P_B(\sigma_B) f(\sigma_A, \sigma_B). \quad (2.3)$$

The limits for σ integrals will be assumed to be over the quadrant $[0, \infty) \times [0, \infty)$ from now on. The weight average molecular weight of block α is $M_{w\alpha} = \langle N_\alpha^2 \rangle_\sigma / \bar{N}_\alpha = \bar{N}_\alpha \langle \sigma_\alpha^2 \rangle_\sigma$. The measure of the polydispersity from Chapter 1 is then $\kappa_\alpha = \langle \sigma_\alpha^2 \rangle_\sigma - 1 = \langle (\sigma_\alpha - 1)^2 \rangle_\sigma$.

There are two polydispersity distributions that will be considered here. The first is the Schultz-Zimm distribution [Zim48]

$$P(\sigma) = \frac{k^k}{\Gamma(k)} \sigma^{k-1} e^{-k\sigma}, \quad (2.4)$$

and the second is a perturbative expansion of a general distribution in terms of the

first three moments about the mean (so the first moment is 0)

$$P(\sigma) = \delta(\sigma - 1) + \frac{1}{2}\kappa\delta''(\sigma - 1). \quad (2.5)$$

where $\delta(\sigma - 1)$ is the usual Dirac delta function. The second moment of (2.4) $\langle(\sigma - 1)^2\rangle_\sigma$ is the polydispersity

$$\kappa = \frac{1}{k}. \quad (2.6)$$

The Schultz-Zimm distribution is graphed in Figure 2.1 for various values of k . It has the nice properties of being highly peaked for large k (small κ), being entirely contained in $\sigma > 0$ (as opposed to a Gaussian distribution), and approaches an exponential distribution for $\kappa \rightarrow 1$, which is seen for polymer melts made by condensation-growth techniques.

The perturbative expansion (2.5) will allow for simpler (and faster) numerical calculations. Whereas the Schultz-Zimm distribution will in general require numerical integrations of equations of the form (2.3), the perturbative distribution (2.5) converts these into

$$\langle f(\sigma_A, \sigma_B) \rangle_\sigma = f(1, 1) + \frac{1}{2}\kappa_A \left. \frac{\partial^2 f}{\partial \sigma_A^2} \right|_{\sigma_A=\sigma_B=1} + \frac{1}{2}\kappa_B \left. \frac{\partial^2 f}{\partial \sigma_B^2} \right|_{\sigma_A=\sigma_B=1}. \quad (2.7)$$

2.2 Self-consistent field theory

We first make a model of the the polymer blend. As before, the block lengths (or degree of polymerization) of the α block will be $N_\alpha(\sigma)$ for a polymer with polymerization index $\sigma = (\sigma_A, \sigma_B)$. Each block will have an associated statistical length of b_α (these will be taken to be equal later)¹. The polymer molecules will

¹The statistical length can be thought of as the size of the coarse-graining in the Gaussian model. Related to it are the persistence length, which is the integral width of the orientational correlation function [Str97], and the Kuhn length b_K , found from assuming the maximum size of the polymer is $R_{max} = Nb_K$, and the average of the square of the end-to-end distance is $R_{ee}^2 = Nb_K^2$.

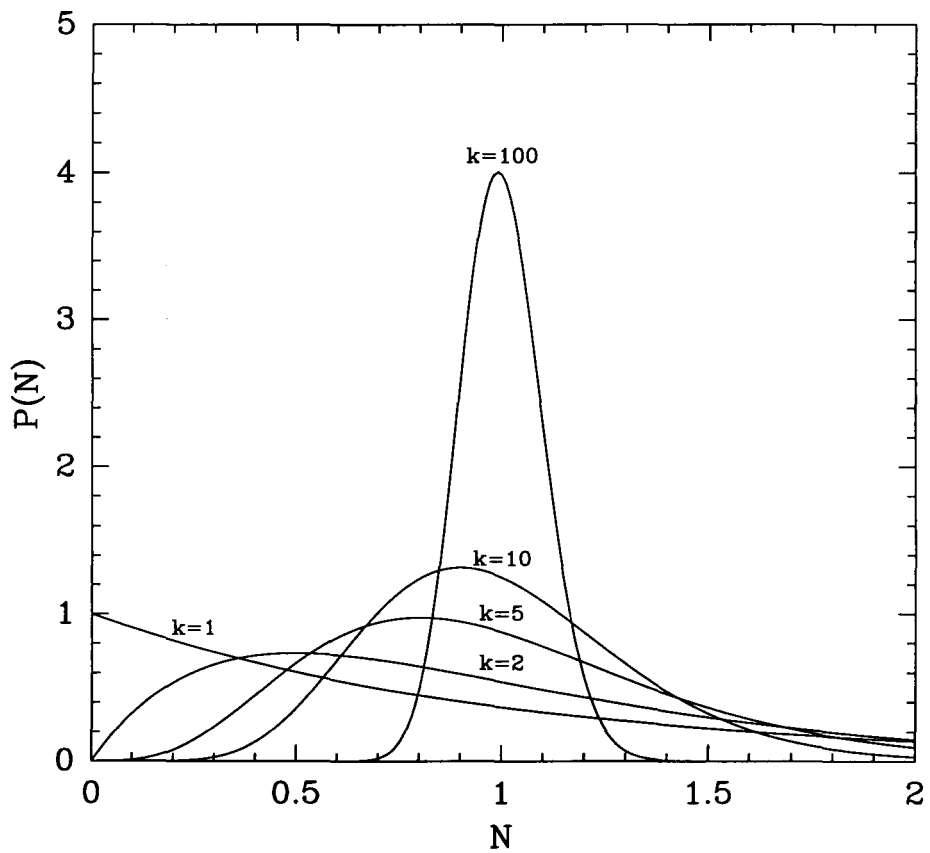


Figure 2.1: Schultz-Zimm distribution for various values of k .

be represented by space curves $R_{\sigma,j}(s)$, where s is the arc length along the curve, and $j = 1, \dots, n_\sigma$ is an index over the set of polymer molecules of type σ (and hence, every molecule is uniquely labelled by σ and j). To simplify the equations, a structure function $\gamma_{\alpha,\sigma}(s)$ will be defined:

$$\gamma_{\alpha,\sigma}(s) = \begin{cases} 1, & \text{if the monomer at } R_{\sigma,j}(s) \text{ is of type } \alpha \\ 0, & \text{otherwise.} \end{cases} \quad (2.8)$$

For simplicity, $\gamma_{\alpha,\sigma}(s) = 0$ for values of s outside of $[0, N(\sigma)]$. Since only one monomer can exist at any given point at one time,

$$\sum_{\alpha} \gamma_{\alpha,\sigma}(s) = 1 \text{ or } 0, \forall \sigma, s. \quad (2.9)$$

The behaviour of $\gamma(s)$ at an interface is undefined; however, this will turn out to be irrelevant. For our diblock copolymer melt, $\gamma_{\alpha,\sigma}(s) = \delta_{A,\alpha}\theta(s - N_A(\sigma)) + \delta_{B,\alpha}\theta(N_B(\sigma) - s)$ where $\theta(x)$ is the Heaviside step function.

A single realisation of the polymer melt is then representable by a set of space curves $\{R_{\sigma,j}(\cdot)\}_{\sigma,j}$ ². Local monomer density operators can be defined as

$$\hat{\rho}_{\alpha}(\mathbf{r}) = \int d\sigma P(\sigma) \sum_j^{n_\sigma} \int_0^{N(\sigma)} ds \delta(\mathbf{r} - R_{\sigma,j}(s)). \quad (2.10)$$

Volume fractions $\phi_{\alpha}(\mathbf{r})$ can be defined by

$$\hat{\phi}_{\alpha}(\mathbf{r}) \equiv \frac{\hat{\rho}_{\alpha}(\mathbf{r})}{\rho_{0\alpha}}, \quad (2.11)$$

where $\rho_{0\alpha}$ is the specific density of an α monomer (so that $\rho_{0\alpha}^{-1}$ is the volume per

²The raised dot (\cdot) is used in place of an explicit index (such as s) to avoid introducing extraneous variables, and to emphasize the importance of the space curve as a whole, not as a point in space.

monomer). Assuming that $N_\alpha(\sigma) = \bar{N}_\alpha \sigma_\alpha$, n_c polymer molecules will occupy a volume of

$$V = \int d\sigma n_\sigma \sum_\alpha \frac{\bar{N}_\alpha \sigma_\alpha}{\rho_{0\alpha}} = n_c \sum_\alpha \frac{\bar{N}_\alpha}{\rho_{0\alpha}}. \quad (2.12)$$

By defining a reference density ρ_0 such that $\rho_0/\bar{N} = n_c/V$, the average polymerizations \bar{N}_α can be rescaled to $N_\alpha = \frac{\rho_0}{\rho_{0\alpha}} \bar{N}_\alpha$. The sum in (2.12) is then $\rho_{0\alpha}^{-1} \sum_\alpha N_\alpha$, and the density of polymers n_c/V is ρ_0/\bar{N} . From here on, the rescaled N_α will be used.

The potential energy due to the monomers $\{\hat{\phi}_\alpha\}$ is given by the functional $\beta\mathcal{V}\{\hat{\phi}\}$, where $\beta = 1/k_B T$. The form of \mathcal{V} will be considered later. We will use the canonical ensemble, where the volume, density, and temperature are considered fixed. The total energy of the system will be

$$\mathcal{H}\{\mathbf{R}, \mathbf{P}\} = \mathcal{T}_\sigma\{\mathbf{P}_{\sigma,j}(\cdot)\} + \mathcal{V}\{\hat{\phi}\} \quad (2.13)$$

where the first term is the kinetic energy of the system, which depends only on the momentum of the polymer molecules. The canonical partition function \mathcal{Z} is then written by summing $e^{-\beta H}$ over all possible states of the system:

$$\mathcal{Z} = \int \left[\prod_\sigma \prod_{j=1}^{n_\sigma} \mathcal{D}\{\mathbf{R}_{\sigma,j}(\cdot)\} \mathcal{D}\{\mathbf{P}_{\sigma,j}(\cdot)\} \right] \left(\prod_\sigma \frac{1}{n_\sigma!} \mathcal{P}_\sigma\{\mathbf{R}_{\sigma,j}(\cdot)\} \right) e^{-\beta \mathcal{H}\{\mathbf{R}, \mathbf{P}\}}. \quad (2.14)$$

The factors of $1/n_\sigma!$ take care of the indistinguishability of the polymers of the same index, and $\mathcal{P}_\sigma\{\mathbf{R}_{\sigma,j}(\cdot)\}$ is the *a priori* probability that the polymer molecule (σ, j) has the configuration $\mathbf{R}_{\sigma,j}(\cdot)$. As a convention, $\int \prod_j^n dx_j$ will be taken to be the multiple integral $\int \cdots \int dx_1 \cdots dx_n$. Furthermore, there is a difficulty in assigning a meaning to the ill-defined product \prod_σ , as σ is assumed to be continuous. However, if we define this as

$$\prod_\sigma f(\sigma) \equiv e^{\int d\sigma \ln f(\sigma)}, \quad (2.15)$$

this difficulty is averted. This definition is reasonable since the integrand for a functional integral is generally required to be an exponential function for it to converge. The momentum terms can be separated out so that the partition function is $\mathcal{Z} = \mathcal{Z}_T \mathcal{Z}_V$, and $\mathcal{Z}_T = \prod_{\sigma} z_{\sigma}^{n_{\sigma}}$. The part due the potential energy is then

$$\mathcal{Z}_V = \int \left[\prod_{\sigma} \prod_{j=1}^{n_{\sigma}} \mathcal{D}\{R_{\sigma,j}(\cdot)\} \right] \left(\prod_{\sigma} \prod_{j=1}^{n_{\sigma}} \frac{1}{n_{\sigma}!} \mathcal{P}_{\sigma}\{R_{\sigma,j}(\cdot)\} \right) e^{-\beta \mathcal{V}(\hat{\phi})}. \quad (2.16)$$

Since the integrand depends on the realisation $\{R_{\sigma,j}(\cdot)\}$ through the density functional $\hat{\phi}$, the multiple integral does not factor. A standard algebraic trick is to introduce factors equal to one. This can be done here by inserting

$$1 = \int \mathcal{D}\{\phi_{\alpha}\} \delta(\phi_{\alpha}(\mathbf{r}) - \hat{\phi}_{\alpha}(\mathbf{r})) \quad (2.17)$$

into the expression for \mathcal{Z}_V . Furthermore, auxiliary fields $\omega_{\alpha}(\mathbf{r})$ can be introduced [Edw66] by converting the δ function to its integral definition, giving

$$1 = \int \mathcal{D}\{\phi_{\alpha}\} \int_{i\infty} \mathcal{D}\{\omega_{\alpha}\} e^{\int d\mathbf{r} \omega_{\alpha}(\mathbf{r})(\phi_{\alpha}(\mathbf{r}) - \hat{\phi}_{\alpha}(\mathbf{r}))}. \quad (2.18)$$

The range of the ω_{α} integral is along a line in the complex plane from $-i\infty$ to $i\infty$. Note that a change of variables $\omega_{\alpha}(\mathbf{r}) = \omega_{\alpha 0} + \omega'_{\alpha}(\mathbf{r})$ where $\omega_{\alpha 0}$ is an arbitrary complex constant has no effect on the identity. Substituting this into (2.16) and rearranging the order of integration:

$$\begin{aligned} \mathcal{Z}_V = & \int \left[\prod_{\alpha} \mathcal{D}\{\phi_{\alpha}\} \right] \int_{i\infty} \left[\prod_{\alpha} \mathcal{D}\{\omega_{\alpha}\} \right] e^{-\beta \mathcal{V}(\phi) + \sum_{\alpha} \int d\mathbf{r} \omega_{\alpha}(\mathbf{r}) \phi_{\alpha}(\mathbf{r})} \\ & \int \left[\prod_{\sigma} \prod_{j=1}^{n_{\sigma}} \mathcal{D}\{R_{\sigma,j}(\cdot)\} \right] \left(\prod_{\sigma} \frac{1}{n_{\sigma}!} \prod_{j=1}^{n_{\sigma}} \mathcal{P}_{\sigma}\{R_{\sigma,j}(\cdot)\} \right) e^{-\sum_{\alpha} \int d\mathbf{r} \omega_{\alpha}(\mathbf{r}) \hat{\phi}_{\alpha}(\mathbf{r})}. \end{aligned} \quad (2.19)$$

For reference, let the last line be A . Using the definition (2.10) for $\hat{\phi}_\alpha$, the exponential in the integrand of A becomes

$$e^{-\Sigma_\alpha \int d\mathbf{r} \omega_\alpha(\mathbf{r}) \hat{\phi}_\alpha(v\mathbf{r})} = \prod_\sigma \prod_{j=1}^{n_\sigma} e^{-\Sigma_\alpha \int ds \omega_\alpha(\mathbf{R}_{\sigma,j}(s)) \gamma_{\alpha,\sigma}(s)}. \quad (2.20)$$

Then,

$$A = \int \left[\prod_\sigma \mathcal{D}\{\mathbf{R}_\sigma(\cdot)\} \right] \prod_\sigma \frac{1}{n_\sigma!} \left[\mathcal{P}_\sigma\{\mathbf{R}_\sigma(\cdot)\} e^{-\Sigma_\alpha \int ds \omega_\alpha(\mathbf{R}_\sigma(s)) \gamma_{\alpha,\sigma}(s)} \right]^{n_\sigma}. \quad (2.21)$$

In a melt, polymer chains are modelled well by a Gaussian chain model, according to Flory's argument[Flo49] where

$$\mathcal{P}_\sigma\{\mathbf{R}(\cdot)\} = \mathcal{N} e^{-\Sigma_\alpha \frac{3}{2b_\alpha^2} \int ds \left| \frac{d\mathbf{R}(s)}{ds} \right|^2 \gamma_{\alpha,\sigma}(s)}. \quad (2.22)$$

and \mathcal{N} is a normalisation constant. Recall that b_α is the statistical length associated with polymers composed of α monomers. Substituting this into (2.21), and using Stirling's approximation $\ln n! \approx n \ln n - n$, A can be rewritten as

$$A = e^{\int d\sigma n_\sigma [\ln(Q_\sigma\{\omega\})/n_\sigma + 1]}, \quad (2.23)$$

where

$$Q_\sigma\{\omega\} = \int \mathcal{D}\{\mathbf{R}(\cdot)\} e^{-\Sigma_\alpha \int ds \left[\frac{3}{2b_\alpha^2} \left| \frac{d\mathbf{R}(s)}{ds} \right|^2 + \omega_\alpha(\mathbf{R}(s)) \right] \gamma_{\alpha,\sigma}(s)} \quad (2.24)$$

is the partition function for a single polymer chain in external fields $\omega_\alpha(\mathbf{r})$. The total partition function is then

$$\mathcal{Z} = \int \left[\prod_\alpha \mathcal{D}\{\phi_\alpha\} \right] \int_{i\infty} \left[\prod_\alpha \mathcal{D}\{\omega_\alpha\} \right] e^{-\beta \mathcal{F}\{\phi, \omega\}}, \quad (2.25)$$

where

$$\beta\mathcal{F}\{\phi, \omega\} = \beta\mathcal{V}\{\phi\} - \sum_{\alpha} \int d\mathbf{r} \omega_{\alpha}(\mathbf{r})\phi_{\alpha}(\mathbf{r}) - \int d\sigma n_{\sigma} [\ln(Q_{\sigma}\{\omega\}/n_{\sigma}) + 1] \quad (2.26)$$

is a free-energy functional. Again, a constant shift of the auxiliary fields $\omega_{\alpha}(\mathbf{r})$ will have no effect on this quantity.

At this point, no approximation beyond the minor one of Stirling's has been made. Evaluating the functional integrals in (2.25) would be sufficient to completely solve for all interesting static properties. However, in general, the integral (2.25) can not be done exactly, so some approximation must be carried out. A first-order approximation that is valid in practise is a mean-field approximation. While the integral (2.25) is intractable, a saddle-point approximation can be done to find functions $\phi_{\alpha}(\mathbf{r})$ and $\omega_{\alpha}(\mathbf{r})$ which maximise the integrand, or, equivalently, minimise $\mathcal{F}\{\phi, \omega\}$. If the integrand is strongly peaked, this should give a good approximation to \mathcal{Z} . The Helmholtz free energy $F = -k_B T \ln \mathcal{Z}$ is then approximated by $\mathcal{F}\{\phi, \omega\}$. Performing the functional derivative of \mathcal{F} with respect to ω_{α} and setting it to 0 gives

$$\phi_{\alpha}(\mathbf{r}) = - \int d\sigma n_{\sigma} \frac{\delta \ln Q_{\sigma}\{\omega_{\alpha}\}}{\delta \omega_{\alpha}(\mathbf{r})} \quad (2.27)$$

$$\omega_{\alpha}(\mathbf{r}) = \frac{\delta \beta\mathcal{V}\{\phi\}}{\delta \phi_{\alpha}(\mathbf{r})}. \quad (2.28)$$

The functional integral in (2.24) for Q_{σ} can be converted to a differential equation in terms of a Green's function $Q_{\sigma}(\mathbf{r}, t; \mathbf{r}', t')$ [Wie86]

$$\frac{\partial Q_{\sigma}(\mathbf{r}, t; \mathbf{r}', t')}{\partial t} = \sum_{\alpha} \gamma_{\alpha, \sigma}(t) \left[-\frac{b_{\alpha}^2}{6} \nabla_{\mathbf{r}}^2 + \omega_{\alpha}(\mathbf{r}) \right] Q_{\sigma}(\mathbf{r}, t; \mathbf{r}', t'), \quad (2.29)$$

with the initial conditions

$$Q_\sigma(\mathbf{r}, t; \mathbf{r}', t') = \delta(\mathbf{r} - \mathbf{r}'). \quad (2.30)$$

Q_σ is then computed as

$$Q_\sigma = \int d\mathbf{r} d\mathbf{r}' Q_\sigma(\mathbf{r}, 0; \mathbf{r}', N(\sigma)) \quad (2.31)$$

and its first derivative is given by

$$\frac{\delta Q_\sigma}{\delta \omega_\alpha(\mathbf{r}_0)} = \int d\mathbf{r} d\mathbf{r}' \int_0^{N(\sigma)} ds \gamma_{\alpha,\sigma}(s) Q_\sigma(\mathbf{r}, 0; \mathbf{r}_0, s) Q_\sigma(\mathbf{r}_0, s; \mathbf{r}', N(\sigma)). \quad (2.32)$$

There are two contributions to the potential \mathcal{V} . There is an energetic contribution $\mathcal{V}_{\text{inter}}$ from the intermolecular potential, and an entropic contribution \mathcal{V}_0 due to the density fluctuations and compressibility effects. Usually, (as will be done here), incompressibility is postulated

$$\sum_\alpha \phi_\alpha(\mathbf{r}) = 1. \quad (2.33)$$

This can be included into the partition function by introducing a δ function

$$\mathcal{Z} = \int \left[\prod_\alpha \mathcal{D}\{\phi_\alpha\} \right] \int_{i\infty} \left[\prod_\alpha \mathcal{D}\{\omega_\alpha\} \right] \delta\left(\sum_\alpha \phi_\alpha - 1\right) e^{-\beta\mathcal{F}\{\phi,\omega\}}. \quad (2.34)$$

By introducing a Lagrange multiplier field $\eta(\mathbf{r})$ coupled to the incompressibility constraint in the same manner as (2.18), the constraint can be moved into the potential as the effective potential

$$\mathcal{V}_0\{\phi\} = \int d\mathbf{r} \eta(\mathbf{r}) \left(\sum_\alpha \phi_\alpha(\mathbf{r}) - 1 \right). \quad (2.35)$$

The interaction potential is usually modelled as a two-body interaction between monomers. In terms of the density fields, this is

$$\beta\mathcal{V}_{\text{inter}}\{\phi\} = \frac{1}{2} \sum_{\alpha,\beta} \int d\mathbf{r} \int d\mathbf{r}' \phi_{\alpha}(\mathbf{r}) \beta V_{\alpha\beta}(\mathbf{r} - \mathbf{r}') \phi_{\beta}(\mathbf{r}'). \quad (2.36)$$

The simplest non-trivial potential is a point interaction: $\beta V_{\alpha\beta}(\mathbf{r}) = \chi_{\alpha\beta} \delta(\mathbf{r})$, where $\chi_{\alpha\beta}$ are called the ‘‘Flory-Huggins’’ parameters. The interaction potential then simplifies to

$$\beta\mathcal{V}_{\text{inter}}\{\phi\} = \frac{1}{2} \sum_{\alpha,\beta} \int d\mathbf{r} \chi_{\alpha\beta} \phi_{\alpha}(\mathbf{r}) \phi_{\beta}(\mathbf{r}). \quad (2.37)$$

For a diblock melt, using the transformation

$$\chi = \chi_{AB} - \frac{1}{2} (\chi_{AA} + \chi_{BB}), \quad (2.38)$$

allows us to write the interaction as

$$\beta\mathcal{V}_{\text{inter}}\{\phi\} = \int d\mathbf{r} \chi \phi_A(\mathbf{r}) \phi_B(\mathbf{r}) + \frac{1}{2} \sum_{\alpha} \chi_{\alpha\alpha} \bar{\phi}_{\alpha} V, \quad (2.39)$$

after using the incompressibility condition $\sum_{\beta} \phi_{\beta}(\mathbf{r}) = 1$.

The self-consistent free-energy density per polymer for the polydisperse diblock melt is then

$$\begin{aligned} \frac{\beta F \bar{N}}{V} = & \sum_{\alpha} \mu_{0\alpha} \bar{\phi}_{\alpha} + \int \frac{d\mathbf{r}}{V} \chi \bar{N} \phi_A(\mathbf{r}) \phi_B(\mathbf{r}) + \int \frac{d\mathbf{r}}{V} \bar{N} \eta(\mathbf{r}) \left[\sum_{\alpha} \phi_{\alpha}(\mathbf{r}) - 1 \right] \\ & - \int \frac{d\mathbf{r}}{V} \sum_{\alpha} \bar{N} \omega_{\alpha}(\mathbf{r}) \phi_{\alpha}(\mathbf{r}) - \int d\sigma \frac{n_{\sigma} \bar{N}}{V} \ln(Q_{\sigma}\{\omega\}/V), \end{aligned} \quad (2.40)$$

where

$$\mu_{0\alpha} = \frac{1}{2} \chi_{\alpha\alpha} \bar{N} + \int d\sigma \frac{n_{\sigma} \bar{N}}{V} \ln(n_{\sigma} V/e). \quad (2.41)$$

By choosing the unit of length for measuring the polymerizations as \bar{N} , the factors of \bar{N} can be absorbed into the auxiliary fields. Additionally, by using $n_c/V = \rho_0/\bar{N}$, and tacitly assuming all space integrals are scaled by the volume of integration, the final result is

$$\frac{\beta F \bar{N}}{V} = \sum_{\alpha} \mu_{0\alpha} \bar{\phi}_{\alpha} + \int d\mathbf{r} \chi \bar{N} \phi_A(\mathbf{r}) \phi_B(\mathbf{r}) - \int d\mathbf{r} \sum_{\alpha} \omega_{\alpha}(\mathbf{r}) \phi_{\alpha}(\mathbf{r}) - \langle \ln Q_{\sigma}(\omega) \rangle_{\sigma}, \quad (2.42)$$

where the $\eta(\mathbf{r})$ has been dropped due to the incompressibility condition, and

$$\mu_{0\alpha} = \frac{1}{2} \chi_{\alpha\alpha} \bar{N} + \langle \ln P(\sigma) / \bar{N} \rangle_{\sigma} - 1. \quad (2.43)$$

The only dependencies on \bar{N} are now in $\mu_{0\alpha}$ and as the single combined Flory-Huggins parameter $\chi \bar{N}$. Using the mean-field equations (2.28) for the fields gives

$$\omega_A(\mathbf{r}) = \chi \bar{N} (\phi_B(\mathbf{r}) - \bar{\phi}_B) + \eta(\mathbf{r}) \quad (2.44)$$

$$\omega_B(\mathbf{r}) = \chi \bar{N} (\phi_A(\mathbf{r}) - \bar{\phi}_A) + \eta(\mathbf{r}), \quad (2.45)$$

where $\eta(\mathbf{r})$ is determined by enforcing the incompressibility condition $\phi_A(\mathbf{r}) + \phi_B(\mathbf{r}) = 1$. In addition, the average of the fields $\int d\mathbf{r} \omega_{\alpha}(\mathbf{r})$ is taken to be zero by introducing a constant shift, as allowed by the argument on page 16 (which also holds for $\eta(\mathbf{r})$). The volume fractions $\phi_{\alpha}(\mathbf{r})$ are determined from (2.27) and (2.32). Instead of using the Green's function $Q_{\sigma}(\mathbf{r}, t; \mathbf{r}', t')$, it is more convenient to use the end-integrated distributions

$$q_{\sigma}(\mathbf{r}, t) = \int d\mathbf{r}' Q_{\sigma}(\mathbf{r}', 0; \mathbf{r}, t) \quad q_{\sigma}^{\dagger}(\mathbf{r}, t) = \int d\mathbf{r}' Q_{\sigma}(\mathbf{r}, N(\sigma) - t; \mathbf{r}', N(\sigma)). \quad (2.46)$$

The relevant quantities to be calculated are the single-chain partition functions Q_{σ} , and their functional derivative with respect to the field $\delta Q_{\sigma} / \delta \omega_{\alpha}(\mathbf{r})$. Q_{σ} is given

in terms of the end-segment distributions $q_\sigma(\mathbf{r}, t)$, and $q_\sigma^\dagger(\mathbf{r}, t)$ as

$$Q_\sigma = \int d\mathbf{r} q_\sigma(\mathbf{r}, N(\sigma)) \quad (2.47)$$

and the functional derivatives are

$$\frac{\delta Q_\sigma}{\delta \omega_A(\mathbf{r})} = \int_0^{N_A(\sigma)} dt q_\sigma(\mathbf{r}, t) q_\sigma^\dagger(\mathbf{r}, N(\sigma) - t) \quad (2.48)$$

$$\frac{\delta Q_\sigma}{\delta \omega_B(\mathbf{r})} = \int_0^{N_B(\sigma)} dt q_\sigma(\mathbf{r}, N(\sigma) - t) q_\sigma^\dagger(\mathbf{r}, t) \quad (2.49)$$

The end-segment distributions are given by

$$q_\sigma(\mathbf{r}, t) = \begin{cases} q_{A\sigma}(\mathbf{r}, t), & t < N_A(\sigma) \\ q_{B\sigma}(\mathbf{r}, t), & t > N_A(\sigma) \end{cases} \quad (2.50)$$

$$q_\sigma^\dagger(\mathbf{r}, t) = \begin{cases} q_{B\sigma}^\dagger(\mathbf{r}, t), & t < N_B(\sigma) \\ q_{A\sigma}^\dagger(\mathbf{r}, t), & t > N_B(\sigma) \end{cases} \quad (2.51)$$

where $q_{\alpha\sigma}$ and $q_{\alpha\sigma}^\dagger$ are both solutions of the modified diffusion equation

$$\frac{\partial q_{\alpha\sigma}}{\partial t} = \left[\frac{b_\alpha^2}{6} \nabla^2 - \omega_\alpha(\mathbf{r}) \right] q_{\alpha\sigma}(\mathbf{r}, t), \quad (2.52)$$

with

$$q_{A\sigma}(\mathbf{r}, 0) = 1 \quad (2.53)$$

$$q_{B\sigma}(\mathbf{r}, N_A(\sigma)) = q_{A\sigma}(\mathbf{r}, N_A(\sigma)) \quad (2.54)$$

$$q_{A\sigma}^\dagger(\mathbf{r}, N_B(\sigma)) = q_{B\sigma}^\dagger(\mathbf{r}, N_B(\sigma)) \quad (2.55)$$

$$q_{B\sigma}^\dagger(\mathbf{r}, 0) = 1. \quad (2.56)$$

For a homogeneous melt (i.e., no structure), $\phi_\alpha(\mathbf{r}) = \bar{\phi}_\alpha$. From (2.44), the auxiliary fields are then zero. The free energy per unit volume per polymer in the homogeneous melt $\beta F_H \bar{N}/V = \beta f_H$ is

$$\beta f_H = \sum_{\alpha} \mu_{0\alpha} \bar{\phi}_\alpha + \chi \bar{N} \bar{\phi}_A \bar{\phi}_B. \quad (2.57)$$

The difference in free-energy density for an inhomogeneous melt from that of the homogeneous is then

$$\beta \Delta f = \chi \bar{N} \int d\mathbf{r} (\phi_A(\mathbf{r})\phi_B(\mathbf{r}) - \bar{\phi}_A \bar{\phi}_B) - \sum_{\alpha} \int d\mathbf{r} \omega_{\alpha}(\mathbf{r})\phi_{\alpha}(\mathbf{r}) - \langle \ln Q_{\sigma}(\omega) \rangle_{\sigma}. \quad (2.58)$$

The only phenomenological parameter left is $\chi \bar{N}$.

Chapter 3

Random Phase Approximation

The true critic is a scrupulous avoider of formulae; he refrains from statements which pretend to be literally true; he finds fact nowhere and approximation always.

T.S. Eliot

Self-consistent field theory, as presented in the previous chapter, is a mean-field theory, i.e., it produces the zeroth-order solution (corresponding to the first correlation function $\langle\phi(\mathbf{r})\rangle$). Self-consistent expansion around the exact mean-field solution allows the effects of higher-order terms to be determined. In particular, the lowest correction to the mean-field solution is in the form of Gaussian fluctuations, corresponding to the density-density correlation functions $\langle\phi(\mathbf{r})\phi(\mathbf{r}')\rangle$. These correlation functions can be obtained with the random phase approximation (RPA) [Doi97, SND96]. For the homogeneous phase, the RPA is a simple extension that is solvable analytically. For fluctuations in the the non-homogeneous monodisperse phases see [SND96, Shi99].

The RPA was used by Hong and Noolandi to examine the structure factors for polydisperse diblock copolymer melts [HN84]. They considered a blend of two copolymers of different lengths, and a melt where the polymer lengths followed the Schultz-Zimm distribution. They assumed only one polydispersity index; given

the index σ , the lengths of the corresponding A and B blocks are $\bar{N}_A\sigma$ and $\bar{N}_B\sigma$, so the total length is $\bar{N}\sigma$. This introduces an unrealistic correlation between the two block lengths, as in reality there is no mechanism during the polymer growth that enforces the A and B blocks on a given polymer to grow such that $N_A/N_B = \bar{N}_A/\bar{N}_B$. However, this assumption gives the same results as assuming uncorrelated block lengths.

The Gaussian correlation function can be used to find the spinodal line for the disorder-to-order transition, and also to locate the critical point. Within RPA, the correlation function is obtained by approximating the structure factor of the system using the non-interacting structure factors. This requires the mean-field solution $\phi_\alpha(r)$, which, while requiring extensive computation for non-homogeneous phases, is trivially the average volume fraction $\bar{\phi}_\alpha$ for the homogeneous phase. It is this phase that will be considered here.

We first assume that the chains are non-interacting (i.e. ignoring excluded volume effects and the incompressibility constraint). The structure factor $\langle \delta\phi_\alpha(r)\delta\phi_\beta(r') \rangle$ will then be that of an ideal polymer melt $S_{\alpha\beta}^0(r-r')$. If this melt is acted upon by external fields $u_\beta(r)$, then by linear response theory,

$$\overline{\delta\phi_a(r)} = -\beta \sum_b \int dr' S_{ab}^0(r-r')u_b(r'). \quad (3.1)$$

The Fourier transform of this is

$$\overline{\phi_a(q)} = -\beta \sum_b S_{ab}^0(q)u_b(q). \quad (3.2)$$

In matrix form, where $\phi = [\overline{\phi_A(q)}, \overline{\phi_B(q)}]^\top$, $u = [u_A(q), u_B(q)]^\top$, and S^0 is the matrix associated with S^0 ,

$$\phi = -\beta S^0 u. \quad (3.3)$$

Now, include incompressibility by adding a field $\eta(r)$ which acts equally on all monomers

$$\phi = -\beta S^0 (u + \eta a), \quad (3.4)$$

where $a = [1, 1]^T$. The incompressibility condition can be written as $a^T \phi = 0$, so solving for η gives

$$\eta = -\frac{a^T S^0 u}{a^T S^0 a}. \quad (3.5)$$

Substituting this back into (3.4) allows us to define an incompressible structure factor S^{inc} which satisfies $\phi = -\beta S^{\text{inc}} u$. This is

$$S^{\text{inc}} = S^0 - \frac{S^0 a a^T S^0}{a^T S^0 a}. \quad (3.6)$$

By multiplying by a on the right and factoring out $S^0 a$ on the left we can see that $S^{\text{inc}} a = 0$, hence S^{inc} is singular, and the rows (and columns) add to 0.

Now we consider the monomer interaction fields $\omega_a(r)$. These couple linearly to the monomer densities as $\omega_a(r) = -\sum_b \chi_{ab} \phi_b(r)$. The matrix version is $\omega = -\chi \phi$. Adding these fields to the external fields gives

$$\phi = -\beta S^{\text{inc}} (u - \chi \phi) \quad (3.7)$$

Solving for ϕ gives the RPA structure factor

$$S^{\text{RPA}} = [I + S^{\text{inc}} \chi]^{-1} S^{\text{inc}}. \quad (3.8)$$

For a two-component system, the incompressible structure factor is

$$S^{\text{inc}} = \frac{S_{AA}^{(0)} S_{BB}^{(0)} - S_{AB}^{(0)2}}{S_{AA}^{(0)} + 2S_{AB}^{(0)} + S_{BB}^{(0)}} \begin{bmatrix} 1 & -1 \\ -1 & 1 \end{bmatrix} \quad (3.9)$$

Letting the prefactor be S^{inc} , the RPA structure factor is then

$$\frac{1}{S} = \frac{1}{S^{\text{inc}}} - 2\chi\bar{N}, \quad (3.10)$$

where the structure factors have been scaled to remove their \bar{N} dependence, and the components of S are $S_{AA} = S_{BB} = -S_{AB} = -S_{BA} = S$.

The individual non-interacting monomer structure factors will be the average of the polymer structure factors, where the individual polymers will be Gaussian chains.

$$S_{AA}^{(0)}(q; \sigma_A, \sigma_B) = \frac{\bar{N}}{N_A} \int_0^{N_A} dn \int_0^{N_A} dm \exp\left(-\frac{b^2}{6}q^2 |n - m|\right) \quad (3.11)$$

$$= \frac{1}{f_A\sigma_A} \int_0^{f_A\sigma_A} dn \int_0^{f_A\sigma_A} dm \exp(-x |n - m|) \quad (3.12)$$

$$\equiv \frac{1}{f_A\sigma_A} S_D(f_A\sigma_A, x), \quad (3.13)$$

where $x = q^2 R_g^2 = q^2 N b^2 / 6$, and

$$S_D(f, x) = \frac{2}{x^2} (fx + e^{-fx} - 1) \quad (3.14)$$

is the Debye structure factor. Similarly, $S_{BB}^{(0)}(q; \sigma_A, \sigma_B) = (1/f_B\sigma_B)S_D(f_B\sigma_B, x)$, and

$$S_{AB}^{(0)}(q; \sigma_A, \sigma_B) = \frac{\bar{N}}{N} \int_0^{N_A} dn \int_{N_A}^N dm \exp\left(-\frac{b^2}{6}q^2 |n - m|\right) \quad (3.15)$$

$$= \frac{1}{f_A\sigma_A + f_B\sigma_B} \frac{1}{2} [S_D(f_A\sigma_A + f_B\sigma_B, x) - S_D(f_A\sigma_A, x) - S_D(f_B\sigma_B, x)]. \quad (3.16)$$

The total non-interacting structure factors are then the averages

$$S_{AA}^{(0)}(x) = \left\langle f_A \sigma_A S_{AA}^{(0)}(x; \sigma_A, \sigma_B) \right\rangle_{\sigma} \quad (3.17)$$

$$S_{BB}^{(0)}(x) = \left\langle f_B \sigma_B S_{BB}^{(0)}(x; \sigma_A, \sigma_B) \right\rangle_{\sigma} \quad (3.18)$$

$$S_{AB}^{(0)}(x) = \left\langle (f_A \sigma_A + f_B \sigma_B) S_{AB}^{(0)}(x; \sigma_A, \sigma_B) \right\rangle_{\sigma}, \quad (3.19)$$

weighted by the relative size of the blocks, as the structure factors are monomer structure factors, and hence the contribution from each block will be proportional to their lengths. Noting that

$$\langle S_D(f_A \sigma_A + f_B \sigma_B, x) \rangle_{\sigma} = \frac{2}{x^2} \left(f_A x + f_B x + \left\langle e^{-f_A \sigma_A x} \right\rangle_{\sigma_A} \left\langle e^{-f_B \sigma_B x} \right\rangle_{\sigma_B} - 1 \right), \quad (3.20)$$

it is easy to see that

$$S_{AA}^{(0)}(x) = \frac{2}{x^2} \left[f_A x + \left\langle e^{-f_A \sigma_A x} \right\rangle_{\sigma_A} - 1 \right] \quad (3.21)$$

$$S_{BB}^{(0)}(x) = \frac{2}{x^2} \left[f_B x + \left\langle e^{-f_B \sigma_B x} \right\rangle_{\sigma_B} - 1 \right] \quad (3.22)$$

$$S_{AB}^{(0)}(x) = \frac{1}{x^2} \left[\left\langle e^{-f_A \sigma_A x} \right\rangle_{\sigma_A} - 1 \right] \left[\left\langle e^{-f_B \sigma_B x} \right\rangle_{\sigma_B} - 1 \right] \quad (3.23)$$

All of the dependence on the form of the polydispersity is then contained in the averages $\langle e^{-f \sigma x} \rangle_{\sigma}$. For the three types of polydispersity considered here, they are

$$\langle e^{-f \sigma x} \rangle_{\sigma} = \begin{cases} e^{-fx}, & \text{monodisperse} \\ \left[1 + \frac{1}{2} \kappa (fx)^2 \right] e^{-fx}, & \text{perturbative} \\ (1 + \kappa fx)^{-1/\kappa}, & \text{Schultz-Zimm} \end{cases} \quad (3.24)$$

To illustrate the results, let us consider the symmetric case $f_A = f_B = 1/2$ and

$\kappa_A = \kappa_B = \kappa$, which leads to

$$S^{\text{inc}}(x) = \frac{1}{2} (S_{AA}^{(0)}(x) - S_{AB}^{(0)}(x)) \quad (3.25)$$

$$= \frac{1}{2x^2} \left[x + 2 \langle e^{-x\sigma/2} \rangle_\sigma - 2 - \left(\langle e^{-x\sigma/2} \rangle_\sigma - 1 \right)^2 \right] \quad (3.26)$$

This is plotted in Figure 3.1 (as a function of wavevector q). It can be seen from this that the perturbative and the Schultz-Zimm distributions agree closely, the major difference being in the intensity for higher polydispersities. The asymptotic behaviour for both in the limits of $x \rightarrow 0$ and $x \rightarrow \infty$ is the same.

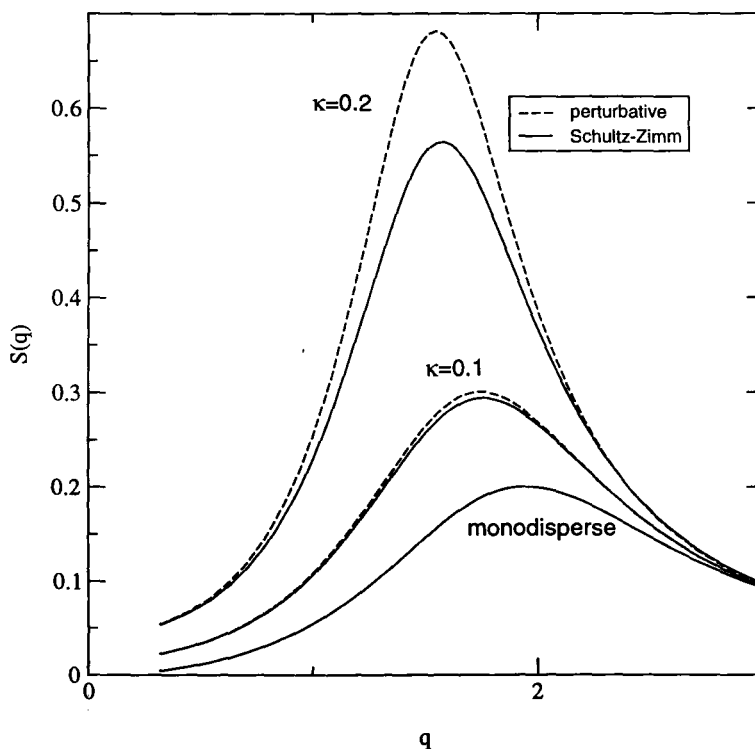


Figure 3.1: Structure factor for the monodisperse case, and for the polydisperse distributions at $f = 0.5$, $\chi N = 8$.

Furthermore, if q^* , the dominant wavevector, is defined as the point at which

$dS(q)/dq = 0$ (and hence $dS^{\text{inc}}(q)/dq = 0$), plotting $S^{\text{inc}}(q)/S^{\text{inc}}(q^*)$ vs. q/q^* gives the results in Figure 3.2. As expected, after accounting for the change in the dominant wavevector, the structure factors are seen to broaden for increasing polydispersity. In addition, the perturbative and Schultz-Zimm distributions are seen to agree even better for $\kappa \leq 0.2$, being almost indistinguishable.

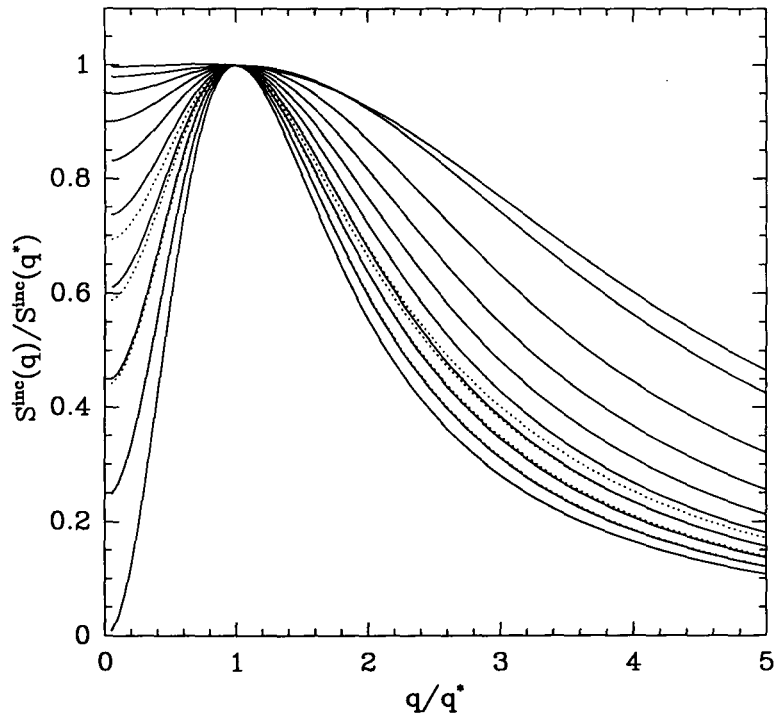


Figure 3.2: Scaled incompressibility-corrected structure factor. Proceeding from inwards outwards, $\kappa = 0$ to $\kappa = 0.9$ in increments of 0.1. The dotted lines are the scaled structure factors for the perturbative distribution; the rest are for the Schultz-Zimm distribution.

The free energy correction with the RPA is

$$F = F^{\text{MFT}} + \frac{1}{2} \int d\mathbf{q} \delta\tilde{\phi}^{\text{T}}(\mathbf{q}) S^{-1}(\mathbf{q}) \delta\tilde{\phi}(\mathbf{q}). \quad (3.27)$$

where F^{MFT} is the mean-field free energy. The spinodal line (where $\partial^2 F / \partial \phi^2 = 0$) is

then where $S^{-1}(q)$ is zero. From (3.10), this is $S^{\text{inc}} = 1/(2\chi N)$.

Figure 3.3 shows the behaviour of the critical point as a function of the polydispersity. The values of χN_c for the perturbative and the Schultz-Zimm distributions are seen to agree reasonable well all the way up to $\kappa = 1$. However, the Schultz-Zimm distribution has $q^* = 0$ at $\kappa = 1$. In the theory of phase transitions, the point at which the magnitude of the critical wavevector goes to zero is called the Lifshitz point. This implies the transition goes from a low symmetry-high symmetry transition to a low symmetry-incommensurate-high symmetry transition, and in this case shows the melt undergoes macrophase separation, such as that found with blends of two incompatible homopolymers. The point $\kappa = 1$ is the same as that found by Angerman [AtBS99] for statistical AB-multiblock copolymers. In addition, at $\kappa = 1$, the critical point for the Schultz-Zimm distribution is at $\chi N_c = 4$, which is the same point that a blend of two homopolymers, each of length $N/2$, would phase separate. Since most diblock copolymers are made by chain-growth polymerization methods with narrow polydispersity $\kappa < 1$, the phase separation at $\kappa = 1$ is not important. However, for those made by step-growth methods (such as some types of polyester diblocks), κ approaches 1 and hence would be poor candidates for applications requiring miscibility [Hie84].

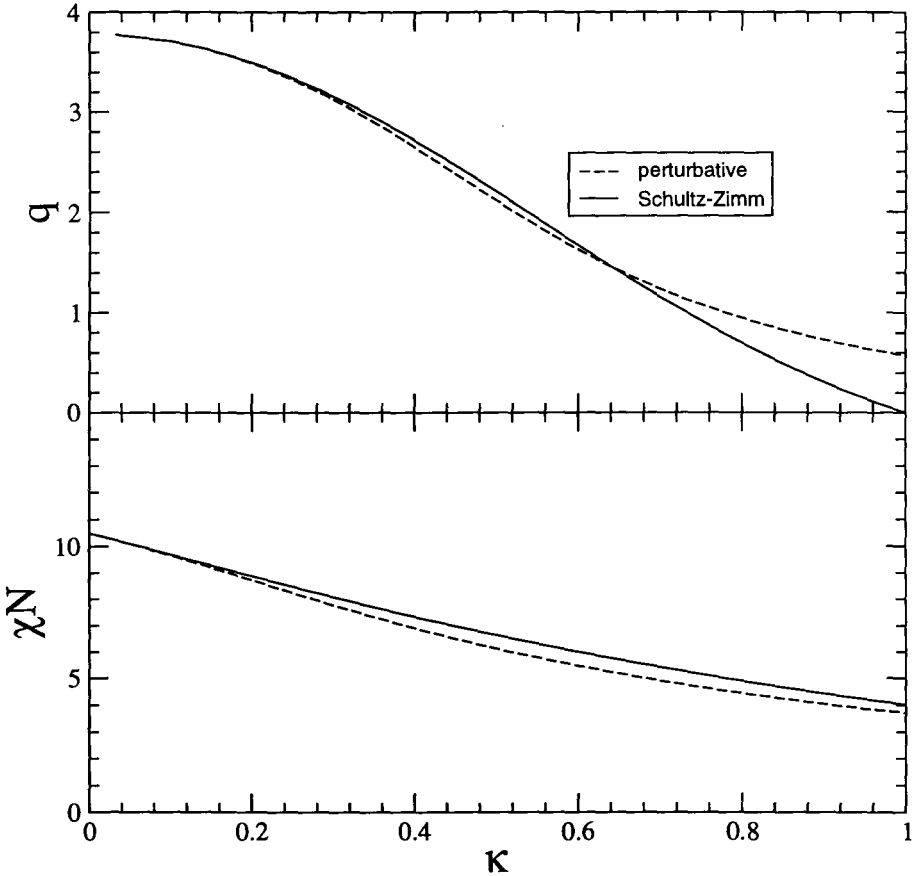


Figure 3.3: Dependence of the position of the critical point on the polydispersity.

Chapter 4

Implementation

If he once again pushes up his sleeves in order to compute for 3 days and 3 nights in a row, he will spend a quarter of an hour before to think which principles of computation shall be most appropriate.

Voltaire, "Diatribes du docteur Akakia"

The SCFT equations (2.27) and (2.28) given in Chapter 2 can not be solved exactly in general. One stumbling block to their solution is that the solutions are functions of the position \mathbf{r} . By an appropriate discretisation, they can be converted to a (large) set of coupled nonlinear equations of scalar variables. Solving the set of equations would, in principle, result in solutions of the ordered structure. However, directly solving the SCFT equations in real space is still formidable task. For ordered structures, there is an efficient method, initially used by Matsen and Schick [MS94], which utilises the symmetrical properties of the phases. The solutions that we are seeking are periodic, since we are looking for ordered phases, which suggests an expansion in a Fourier-like series. The appropriate basis functions for the expansion are the eigenfunctions $f_n(\mathbf{r})$ of the Laplace equation $\nabla^2 f_n(\mathbf{r}) = -\lambda_n^2 f_n(\mathbf{r})$, where λ_n is the eigenvalue corresponding to $f_n(\mathbf{r})$, and with periodic boundary condition where the period is that of the unit cell of the structure being considered. The symmetries of the phase being considered will lead to degeneracies in the basis

functions.

In all of the structures studied here (lamellar, hex, bcc, and gyroid), only one parameter D is required to describe the period of the structure. In this case, $\lambda_n \propto 1/D$. In general, λ_n is the length of a reciprocal lattice vector associated with the basis function $f_n(\mathbf{r})$; this is explained in more detail in Appendix A. For an orthogonal, cubic, basis, $\lambda_n = 2\pi/D \sqrt{h^2 + k^2 + l^2}$, where (h, k, l) are the Miller indices of the related reciprocal lattice vector.

By convention, $f_0(\mathbf{r}) = 1$, and the eigenfunctions are ordered by increasing values of λ_n . In addition, they are taken to be orthonormal, so

$$\int d\mathbf{r} f_n(\mathbf{r})f_m(\mathbf{r}) = \delta_{nm}. \quad (4.1)$$

An arbitrary function with the period of the unit cell can then be expanded in a Fourier-like series

$$g(\mathbf{r}) = \sum_{n=0}^{\infty} g_n f_n(\mathbf{r}). \quad (4.2)$$

The $q_\alpha(\mathbf{r}, t)$, $q_\alpha^\dagger(\mathbf{r}, t)$, and $\omega_\alpha(\mathbf{r})$ are expanded in this way¹. Substituting this expansion into (2.52) gives

$$\frac{\partial q_{\alpha n}(t)}{\partial t} = -\frac{b_\alpha^2 \lambda_n^2}{6} q_{\alpha n}(t) - \sum_{m=0}^{\infty} \sum_{l=0}^{\infty} \omega_{\alpha l} q_{\alpha m}(t) \Gamma_{nml} \quad (4.3)$$

where

$$\Gamma_{nml} = \int d\mathbf{r} f_n(\mathbf{r})f_m(\mathbf{r})f_l(\mathbf{r}). \quad (4.4)$$

The algebra can be made clearer by moving to a vector representation. Let $\mathbf{q}_\alpha(t) = [q_{\alpha 0}(t), q_{\alpha 1}(t), \dots]^\top$, and $\boldsymbol{\omega}_\alpha = [\omega_{\alpha 0}, \omega_{\alpha 1}, \dots]^\top$. Then we can rewrite the above

¹Unless otherwise noted, the subscript σ used for denoting the polymerization index in Chapter 2 will be implied

as

$$\frac{\partial \mathbf{q}_\alpha(t)}{\partial t} = - \left[\frac{b_\alpha^2}{6} \mathbf{D}(\lambda^2) + \Omega_\alpha \right] \mathbf{q}_\alpha(t) \quad (4.5)$$

where $\lambda^2 = [\lambda_0^2, \lambda_1^2, \dots]^\top$, $\mathbf{D}(x)$ is an operator that forms a matrix with x on the diagonal (and is zero everywhere else), and

$$[\Omega_\alpha]_{nm} = \sum_{l=0}^{\infty} \omega_{\alpha l} \Gamma_{nml} \quad (4.6)$$

Let

$$H_\alpha = - \frac{b_\alpha^2 \lambda^2}{6} - \Omega_\alpha \quad (4.7)$$

then (4.5) can be rewritten as the matrix differential equation

$$\frac{d\mathbf{q}_\alpha(t)}{dt} = H_\alpha \mathbf{q}_\alpha(t). \quad (4.8)$$

The solution to this equation is then

$$\mathbf{q}_\alpha(t) = \Phi_\alpha e^{\mathbf{D}(\varepsilon^\alpha(t-t_0))} \Phi_\alpha^\top \mathbf{q}_\alpha(t_0), \quad (4.9)$$

where the columns of Φ_α are the eigenvectors of H_α , and $[\varepsilon^\alpha]_n$ are the corresponding eigenvalues. For simplicity, let $\mathbf{e} = [1, 0, 0, \dots]^\top$. This gives

$$\mathbf{q}_A(t) = \Phi_A \mathbf{D}(e^{\varepsilon^A t}) \Phi_A^\top \mathbf{e} \quad (4.10)$$

$$\mathbf{q}_B(t) = \Phi_B \mathbf{D}(e^{\varepsilon^B(t-N_A)}) \Phi_B^\top \Phi_A \mathbf{D}(e^{\varepsilon^A N_A}) \Phi_A^\top \mathbf{e} \quad (4.11)$$

$$\mathbf{q}_A^\dagger(t) = \Phi_A \mathbf{D}(e^{\varepsilon^A(t-N_B)}) \Phi_A^\top \Phi_B \mathbf{D}(e^{\varepsilon^B N_B}) \Phi_B^\top \mathbf{e} \quad (4.12)$$

$$\mathbf{q}_B^\dagger(t) = \Phi_B \mathbf{D}(e^{\varepsilon^B t}) \Phi_B^\top \mathbf{e}. \quad (4.13)$$

The single-chain partition function is given by Eq. (2.47). Expanding into basis

functions gives

$$\begin{aligned}
 Q &= \sum_{n=0}^{\infty} q_n(N_A + N_B) \int d\mathbf{r} f_n(\mathbf{r}) \\
 &= q_0(N_A + N_B) \\
 &= [\mathbf{q}_B(N_A + N_B)]_0.
 \end{aligned} \tag{4.14}$$

This can be rewritten in our matrix notation as $Q = \mathbf{e}^T \mathbf{q}_B(N_A + N_B)$, and hence

$$Q = \mathbf{e}^T \Phi_B D(\mathbf{e}^{\varepsilon^B N_B}) \Phi_B^T \Phi_A D(\mathbf{e}^{\varepsilon^A N_A}) \Phi_A^T \mathbf{e}, \tag{4.15}$$

which is nicely symmetric. Letting $L = \Phi_B^T \Phi_A$, and $s_\alpha(N_\alpha) = \mathbf{e}^{D(\varepsilon^B N_B)} \Phi_\alpha^T \mathbf{e}$ (note that $[s_\alpha(N_\alpha)]_i = \mathbf{e}^{\varepsilon_i^{\alpha} N_B} \Phi_{\alpha 0 i}$), we have

$$Q = s_B(N_B)^T L s_A(N_A)^T. \tag{4.16}$$

The functional derivatives, in terms of the single-block distributions are

$$\frac{\delta Q}{\delta \omega_A(\mathbf{r})} = \int_0^{N_A} dt q_A(\mathbf{r}, t) q_A^\dagger(\mathbf{r}, N_A + N_B - t) \tag{4.17}$$

$$\frac{\delta Q}{\delta \omega_B(\mathbf{r})} = \int_0^{N_B} dt q_B(\mathbf{r}, N_A + N_B - t) q_B^\dagger(\mathbf{r}, t). \tag{4.18}$$

Note that $\delta Q/\delta \omega_A$ is related to $\delta Q/\delta \omega_B$ by the transformation $A \leftrightarrow B$, $q \leftrightarrow q^\dagger$. We will look at $\delta Q/\delta \omega_A$. Substituting in the expansions for q_A and q_A^\dagger gives

$$\frac{\delta Q}{\delta \omega_A} = \sum_{n,m} \int_0^{N_A} dt q_{An}(t) q_{Am}^\dagger(N_A + N_B - t) f_n(\mathbf{r}) f_m(\mathbf{r}). \tag{4.19}$$

The double basis functions can be removed by multiplying by $f_i(\mathbf{r})$, and integrating

over r . This gives

$$\frac{\delta Q}{\delta \omega_A} = \sum_l [\Gamma^A(B^A)]_l f_l(r), \quad (4.20)$$

where B^A is defined by

$$\Phi_A B_{nm}^A \Phi_A^\top = \int_0^{N_A} dt q_{An}(t) q_{Am}^\dagger (N_A + N_B - t). \quad (4.21)$$

and $\Gamma^\alpha(M)$ is

$$[\Gamma^\alpha(M)]_l = \sum_{nm} [\Phi_\alpha M \Phi_\alpha^\top]_{nm} \Gamma_{nml}. \quad (4.22)$$

Note that $\Gamma^\alpha(M)$ is linear in its argument. Substituting in the solutions for q_A and q_A^\dagger yields

$$B^A = \int_0^{N_A} dt D(e^{\epsilon^A t}) \Phi_A^\top e e^\top \Phi_B D(e^{\epsilon^B N_B}) \Phi_B^\top \Phi_A D(e^{\epsilon^A (N_A - t)}). \quad (4.23)$$

For convenience, let $A^A(N_B) = \Phi_A^\top e e^\top \Phi_B D(e^{\epsilon^B N_B}) L = (\Phi_A^\top e) s_B (N_B)^\top L$. Define $A \odot B$ to be elementwise multiplication of two matrices, so $[A \odot B]_{ij} = A_{ij} B_{ij}$. B^A can then be rewritten using A^A as

$$B^A = \int_0^{N_A} dt D(e^{\epsilon^A t}) A^A(N_B) D(e^{\epsilon^A (N_A - t)}). \quad (4.24)$$

By expanding into components, it can be seen that the integral above can be rewritten as

$$B^A = A^A(N_B) \odot C^A(N_A), \quad (4.25)$$

where $C^A(N_A)$ is given by

$$\begin{aligned} [C^A(N_A)]_{ij} &= \int_0^{N_A} dt e^{\varepsilon_i^A t} e^{\varepsilon_j^A (N_A - t)} \\ &= \begin{cases} \frac{e^{\varepsilon_i^A N_A} - e^{\varepsilon_j^A N_A}}{\varepsilon_i^A - \varepsilon_j^A}, & \varepsilon_i^A \neq \varepsilon_j^A \\ N_A e^{\varepsilon_j^A N_A}, & \varepsilon_i^A = \varepsilon_j^A. \end{cases} \end{aligned} \quad (4.26)$$

Similarly,

$$B^B = A^B(N_A) \odot C^B(N_B) \quad (4.27)$$

$$\frac{\delta Q}{\delta \omega_B} = \sum_l [\Gamma^B(B^B)]_l f_l(\mathbf{r}) \quad (4.28)$$

4.1 Perturbative polydispersity

There are two quantities that need to be averaged when extending the previous results to include polydispersity. These are $\frac{1}{Q} \frac{\delta Q}{\delta \omega_\alpha}$ (for the volume fraction $\phi_\alpha(\mathbf{r})$), and $\ln Q$ (for the free energy). Instead of differentiating with respect to the polydispersity indices σ_α , as used in the perturbative expansion (2.7), derivatives with respect to N_A and N_B will be used, and will be denoted by subscripts, so $Q_{;\alpha} = \partial Q / \partial N_\alpha$ and $Q_{;\alpha\beta} = \partial^2 Q / \partial N_\alpha \partial N_\beta$. Also, let $K = 1/Q$, and $R^\alpha = \delta Q / \delta \omega_\alpha$.

The perturbative expansions of $\frac{1}{Q} \frac{\delta Q}{\delta \omega_\alpha}$ and $\ln Q$ are

$$\left\langle \frac{1}{Q} \frac{\delta Q}{\delta \omega_A} \right\rangle_\sigma = KR^A + \frac{1}{2} \kappa_A N_A^2 (KR^A)_{;AA} + \frac{1}{2} \kappa_B N_B^2 (KR^A)_{;BB} \quad (4.29)$$

and

$$\langle \ln Q \rangle_\sigma = \ln Q + \frac{1}{2} \kappa_A N_A^2 (\ln Q)_{;AA} + \frac{1}{2} \kappa_B N_B^2 (\ln Q)_{;BB}. \quad (4.30)$$

We then have

$$\begin{aligned} \left\langle \frac{1}{Q} \frac{\delta Q}{\delta \omega_A} \right\rangle_\sigma &= KR^A + \frac{1}{2} \kappa_A N_A^2 (K_{,AA} R^A + 2K_{,A} R_{,A}^A + KR_{,AA}^A) \\ &\quad + \frac{1}{2} \kappa_B N_B^2 (K_{,BB} R^A + 2K_{,B} R_{,B}^A + KR_{,BB}^A). \end{aligned} \quad (4.31)$$

From the expansion of $\partial Q / \partial N_\alpha$ in (4.20) and (4.25), and the linearity of $\Gamma^\alpha(M)$, this is just

$$\begin{aligned} \left\langle \frac{1}{Q} \frac{\delta Q}{\delta \omega_A} \right\rangle_\sigma &= \Gamma^A \left(\frac{1}{Q} [A^A(N_B) \odot C^A(N_A)] + \frac{1}{2} k^A A^A \odot [C^A + 2C_{,A}^A + C_{,AA}^A] \right. \\ &\quad \left. + \frac{1}{2} k^B C^A \odot [A^A + 2A_{,B}^A + A_{,BB}^A] \right) \end{aligned} \quad (4.32)$$

where $k^A = N_A^2 \kappa_A K_{,AA}$ and $k^B = N_B^2 \kappa_B K_{,BB}$.

The average of $\ln Q$ is done similarly:

$$\langle \ln Q \rangle_\sigma = -\ln K + \frac{1}{2} \kappa_A N_A^2 \left(\frac{(K_{,A})^2}{K^2} - \frac{K_{,AA}}{K} \right) + \frac{1}{2} \kappa_B N_B^2 \left(\frac{(K_{,B})^2}{K^2} - \frac{K_{,BB}}{K} \right) \quad (4.33)$$

The quantities that need to be calculated are then K , $K_{,\alpha}$, $K_{,\alpha\alpha}$, A^α , $A_{,\beta}^\alpha$, $A_{,\beta\beta}^\alpha$, C^α , $C_{,\alpha}^\alpha$, and $C_{,\alpha\alpha}^\alpha$, where β is B if α is A, and vice versa. The derivatives of A^α and C^α are trivial from their definitions, and those of K ($= 1/Q$) are easily derived from the expansion of Q in (4.16). Note that both A^α and Q are expressible in terms of $s_\alpha(N_\alpha)$, so only the derivatives of $s_\alpha(N_\alpha)$ and $C^\alpha(N_\alpha)$ need to be determined.

Once $\phi_a = \langle \frac{1}{Q} \frac{\delta Q}{\delta \omega_a} \rangle_\sigma$ and $\langle \ln Q \rangle_\sigma$ have been calculated using the above procedure, the SCFT calculation proceeds just as in the monodisperse melt.

Chapter 5

Results and Discussion

Sometimes I've believed as many as six impossible things before breakfast.

Lewis Carroll

Using the methods described in the previous chapter, the free energies of different phases were calculated, and this information was used to construct phase diagrams. Approximately one week of computer time was used, with almost 40 000 points being calculated. A Compaq DS20 workstation with two 667 MHz 21264 Alpha processors with 8 MiB¹ L2 cache running Tru64, along with three desktops (with a PIII 833 MHz, PIII 933 MHz, and an Athlon 1.3 GHz) running Linux were used in the computation. All four machines were roughly equal in how long an individual calculation would run, with the Alpha and the Athlon being the fastest. The program was written in Python[Ros] using the Numerical Python package[Dub] and some custom-written extensions written in C for speed-critical parts. Python, although not a compiled language, was chosen for its ease-of-use, along with its support for modern, high-level programming methodologies, such

¹1 MiB = 1 mebibyte = 1024 kibibyte (KiB), and 1 KiB = 1024 B. These binary prefixes were standardised in December 1998 by the International Electrotechnical Commission (IEC) to prevent confusion with the standard SI metric prefixes. See <http://physics.nist.gov/cuu/Units/binary.html> for more information.

as object-oriented programming. The Numerical Python extensions allow array operations to be performed at speeds close to that of compiled code (similar to MATLAB and other array-based languages), while still maintaining the conciseness and readability of Python. If the Python code is found to be too slow, parts of the code can be rewritten in C (or Fortran) for speed. This way, only those parts which actually need to be fast are rewritten, instead of attempting to perform all tasks in a lower-level language. A rewrite of the entire code base for this thesis in C would gain a small increase in speed at the large expense of maintainability, extensibility, and reusability. As written, the developed code can easily be used for examining other polymeric systems, such as blends of triblocks, with self-consistent field theory.

The phases used were those that have been found to be stable (with SCFT) for the monodisperse case: body-centred cubic (bcc), gyroid, cylindrical (hex), and lamellar (see Figure 1.2). The transition lines between the structured phases were determined by finding the crossing point between the free energies of the two phases using linear interpolation of the data. The order-disorder transition was found by using a parabolic extrapolation, which works well for points away from the critical point where the discontinuity in the first derivative of the free energy is large. However, at the critical point, the free energy is predicted to be parabolic and tangent to this point. Hence, the extrapolated parabolic fit may either not intersect with $\Delta f = 0$, or the intersection point will be ill-defined as the problem of finding the intersection becomes singular. Instead, the RPA value for the critical point was used; this turns out to work well. As an example, the calculated free energy (for $\chi N = 12$) differences from the homogeneous phase for the hex and gyroid phases are presented in Figure 5.1.

One test of the accuracy of the perturbation expansion of the SCFT equations is to compare the bcc-to-homogeneous transition to the spinodal line calculated from the random phase approximation in Chapter 3. The two should agree at the

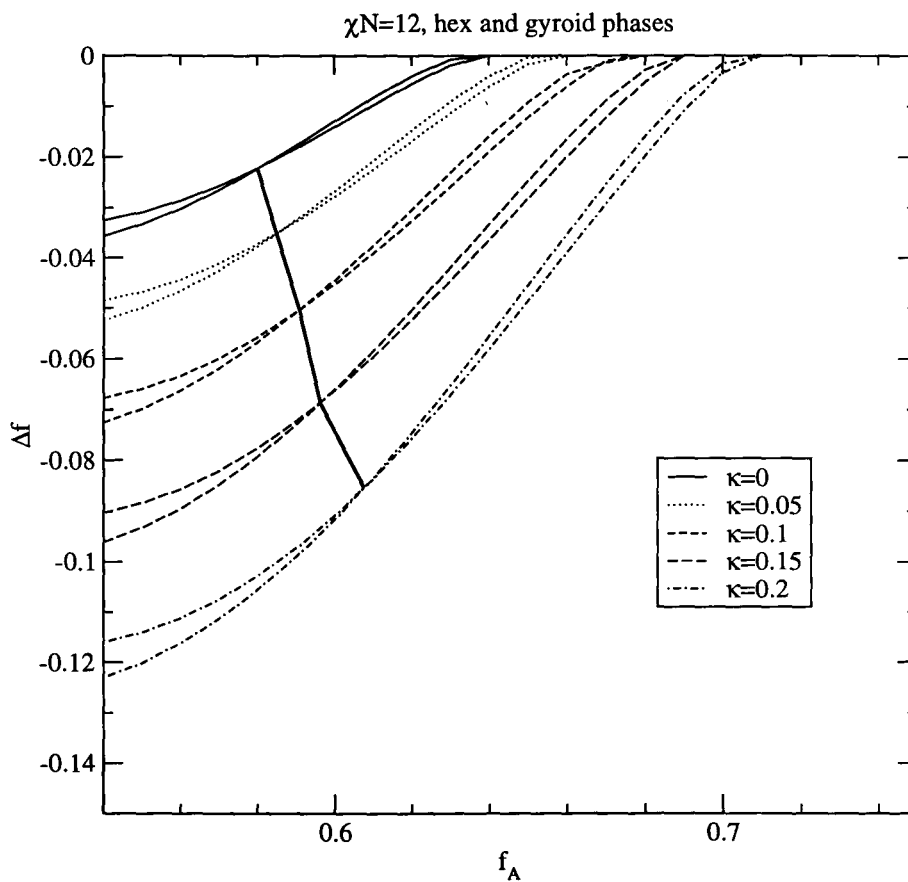


Figure 5.1: Free energy of the hex and gyroid phases. The thick solid line that intersects the free energies denotes the interface between the hex and gyroid phases for each value of κ .

critical point $f = 0.5$, and should be close for values of f near to 0.5. However, since (in mean-field theory) $f = 0.5$ is a critical point, it is difficult to determine it precisely: the convergence of the SCFT equations becomes very slow near it, and extrapolation must be used as the free energy can only be determined on one side of it. The extrapolation (using a parabolic fit, as mentioned above) becomes singular at the critical point, as the first derivative of the free energy is continuous and zero there. Because of these problems, Figure 5.2 shows the order-disorder transition (ODT) for $f = 0.48$, which is sufficiently far away from the critical point for results to be accurately determined, yet close enough to be useful for comparison. We can see that the spinodal calculated from the RPA is in excellent agreement with the ODT as determined from SCFT.

5.1 Phase diagrams

The phase diagrams for different $\kappa_A = \kappa_B$ values are plotted in Figure 5.3. The phase diagrams of these symmetric polydisperse melts are similar to that for the monodisperse melt in Figure 1.1. They are symmetric, parabolic, contain the same phases, have triple points at the intersection of the hex, gyroid, and lamellar phases, and have a critical point at $f_c = 0.5$. The most striking change is the drop in the order-disorder transition to lower χN , and a corresponding drop in the other phase transition lines. The drop in the ODT is also predicted by the RPA. In addition, the range of f for the region of stability for the lamellar phase decreases as κ increases, while the range for the hex phase increases. Also, as κ increases, the transition lines for the lamellar-gyroid and gyroid-hex transitions become less parabolic and closer to being constant as χN increases.

Phase diagrams for one-sided polydisperse melts for $\kappa_A = 0.05, \kappa_B = 0$, and $\kappa_A = 0.15, \kappa_B = 0$ are plotted in Figure 5.4. The asymmetry in the polydispersity breaks the $f_A \leftrightarrow 1 - f_A$ symmetry of the phase diagram. The phase diagrams

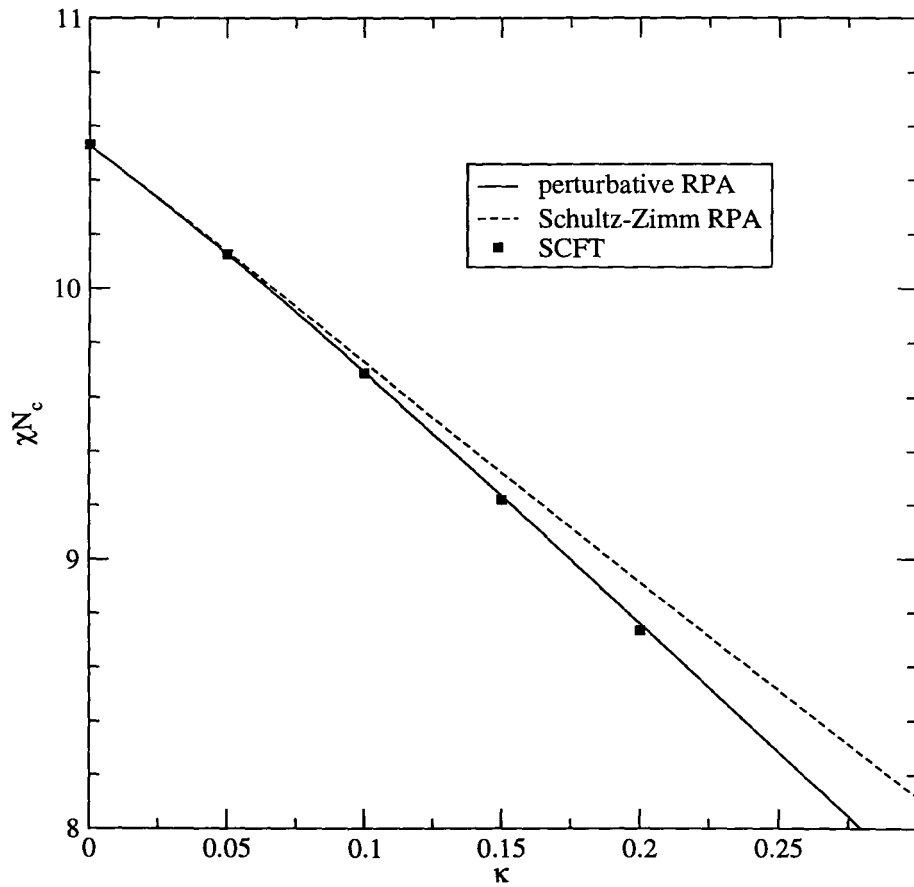


Figure 5.2: Comparison of the ODT as found with SCFT to the spinodal line calculated using the RPA for $f = 0.48$.

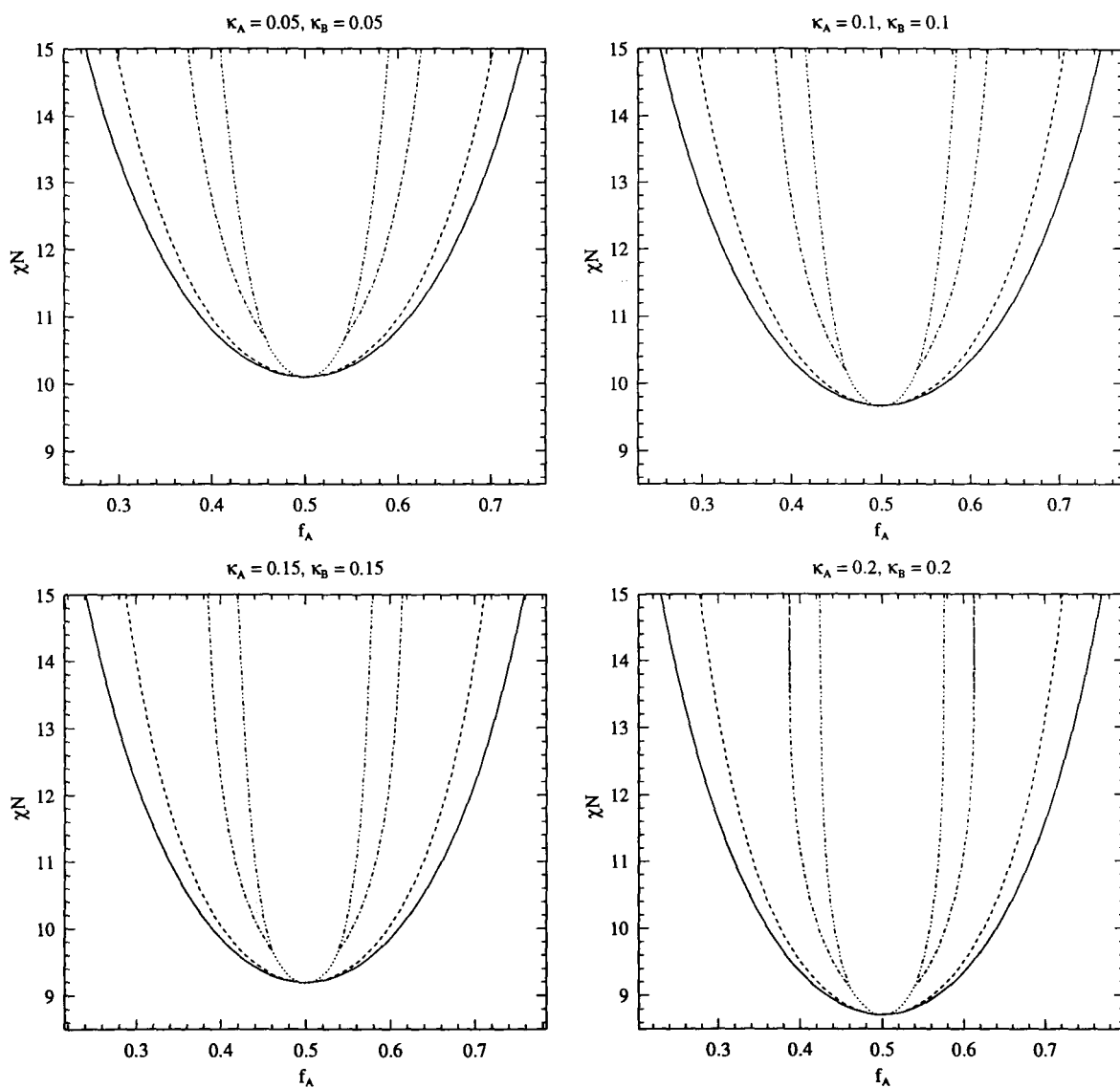


Figure 5.3: Phase diagrams for diblock melts where each block is equally polydisperse. The phases are in the same relative positions as for the monodisperse melt in Figure 1.1

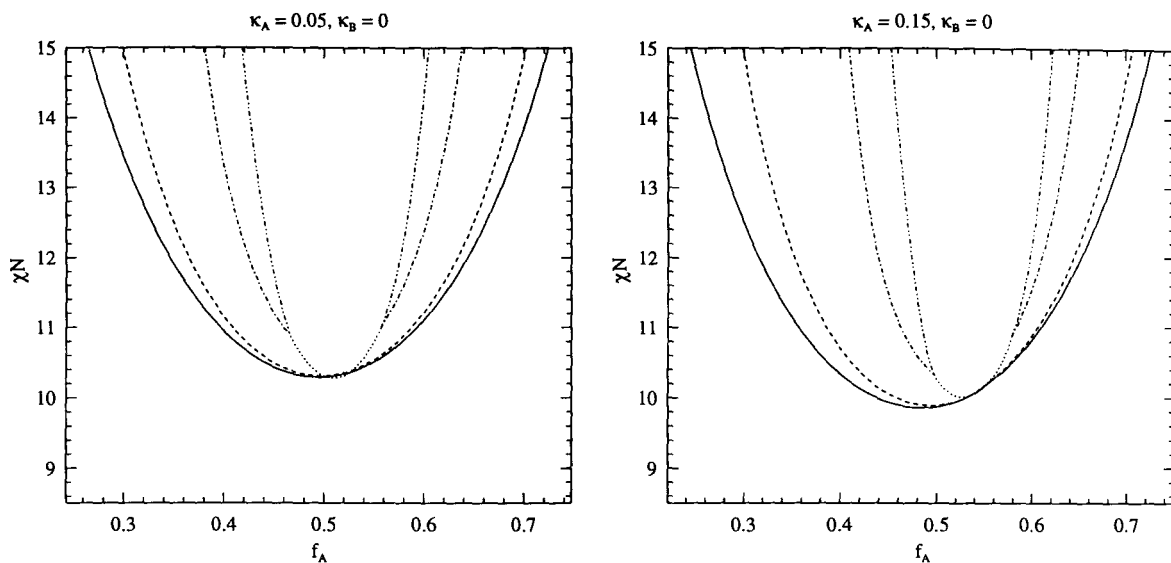


Figure 5.4: Phase diagrams for diblock melts with one block monodisperse.

are compressed toward where the polydisperse block is predominant. However, the transition lines are still roughly parabolic, albeit no longer symmetrical about $f = 0.5$. The critical point has moved up one side of the ODT, instead of being at the minimum χN of the ODT. This is mirrored by the shift in triple points, which are tilted with respect to their monodisperse positions. The regions of stability have changed also; the phases where the polydisperse block is in the minority are stable for a wider range of f for a given χN , while those where the polydisperse block is in the majority are smaller. The drop in the ODT is approximately the same as that for a symmetric polydisperse melt with $\kappa_{\text{sym}} = \frac{1}{2}(\kappa_A + \kappa_B)$, implying the amount of the drop is due to the average of the block polydispersities.

5.2 Periodicity

In addition to the decrease in χN of the transition lines, there is another effect due to polydispersity which is more pronounced. The periods D of each phase for a range of polydispersities are plotted in Figure 5.5 for $\chi N = 12$. In Figure 5.6, the period as a function of χN is plotted for the lamellar phase at $f = 0.5$. From the figures, it is obvious that the period increases with polydispersity. Experimentally, this effect should be easier to observe than the shift in transition points, as periodicity is given by scattering techniques and by direct observation with microscopy. Figure 5.6 shows another experimentally accessible behaviour: the change in the period as a function of χN is less for the more polydisperse melts. Since χN (being approximately proportional to the inverse of the temperature) is easier to change than the block composition, this would be an easier graph to reproduce (although there is a lower limit on reachable values of χN because of the glass transition, and the decomposition temperature of the polymer).

The increase in period for increasing polydispersity is explained by looking at the distribution of the different block lengths in the melt. This is shown for a particular case in Figure 5.7, where the spatial deviations of the A block volume fractions for the deciles of the polymer length distribution from one-tenth of the total volume fraction are graphed. It shows that the longer blocks preferentially occupy the centre of the cylinders, whereas there are hardly any of the shortest blocks there. Between the cylinders, where the B form the bulk, the shortest A blocks have a higher concentration. There are two effects that explain this. A blend of two homopolymers (of the same length, for simplicity) which have a $\chi > 0$ will phase separate when $\chi > 2/N$. Since χ is (roughly) a constant due to the monomer types and not the polymer lengths, this implies that longer polymers are less miscible. Hence, the short A blocks will be energetically more favourable to coexist with the majority B phase than the longer A blocks. Also, for a short A block to be in

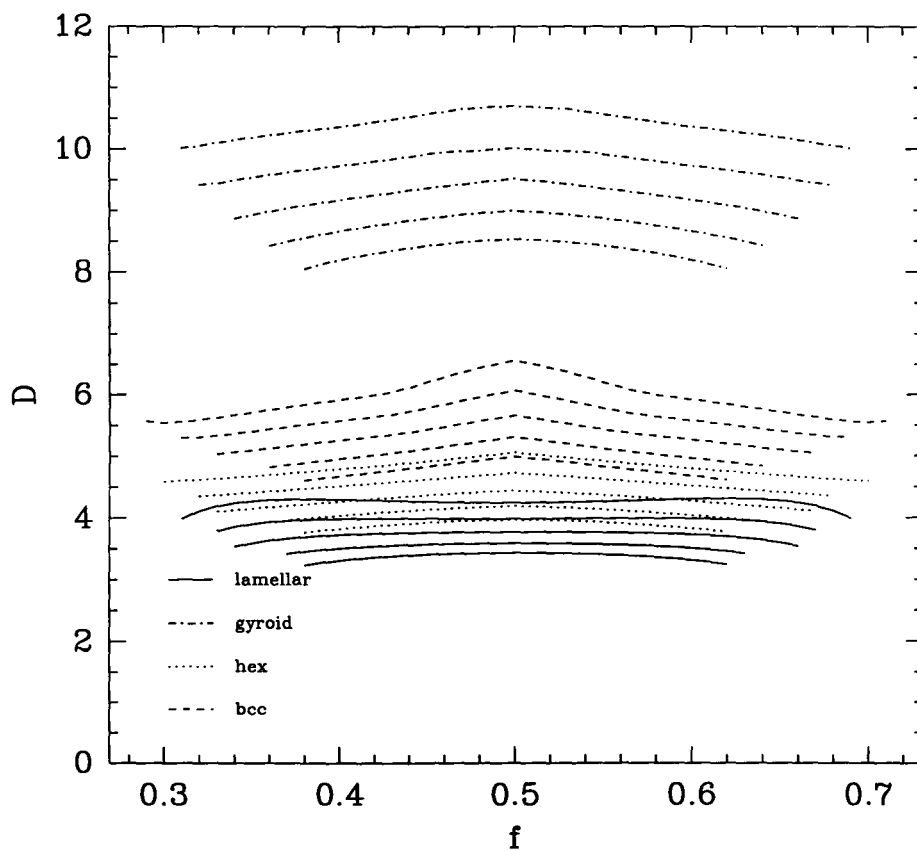


Figure 5.5: Change in period as κ increases for the four phases. For each phase, κ from bottom to top is 0, 0.05, 0.1, 0.15, and 0.2. The value of χN here is 12.

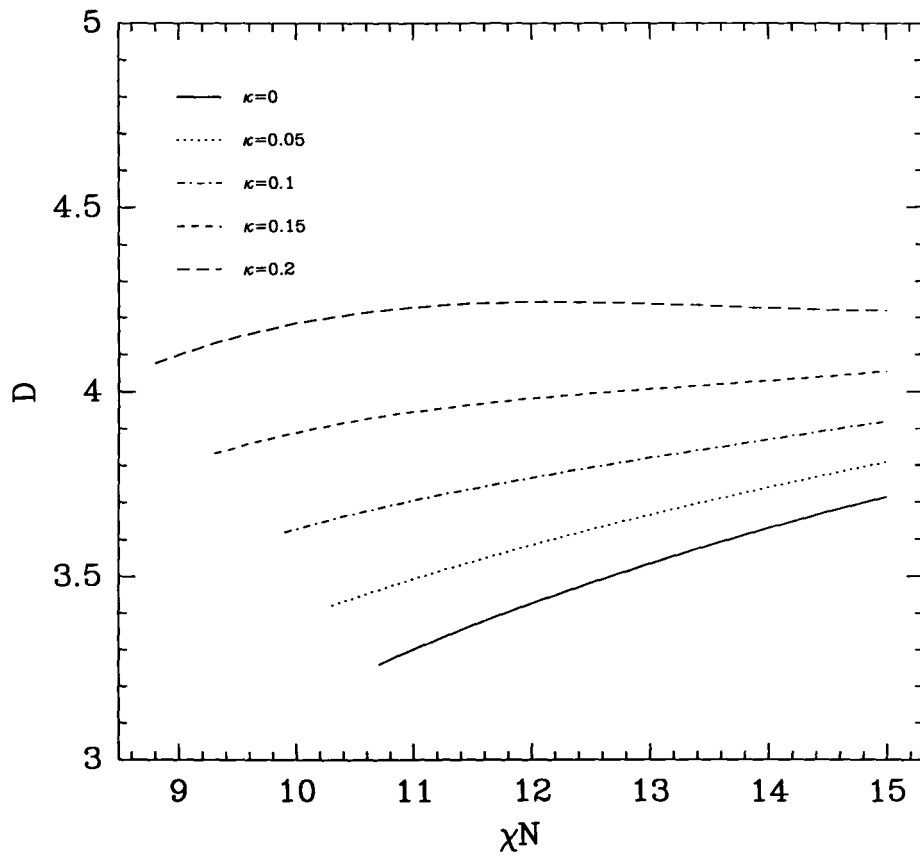


Figure 5.6: A different view of the change in period. Here, the period of the lamellar phase for $f = 0.5$ is shown.

the centre, more of the B block on the same chain must be in a higher concentration of A blocks, which is not favourable. In addition to the energy differences, there is an entropic contribution. When stretched or compressed (from its equilibrium state), the number of configurations available to a polymer molecule goes down, and hence its entropy decreases. At least in a melt, the average density distribution of a single polymer chain will be a Gaussian distribution. For a short A block to be at the centre of one of the cylinders and not to have too much B block also in the cylinder, it would have to be stretched, which is entropically unfavourable.

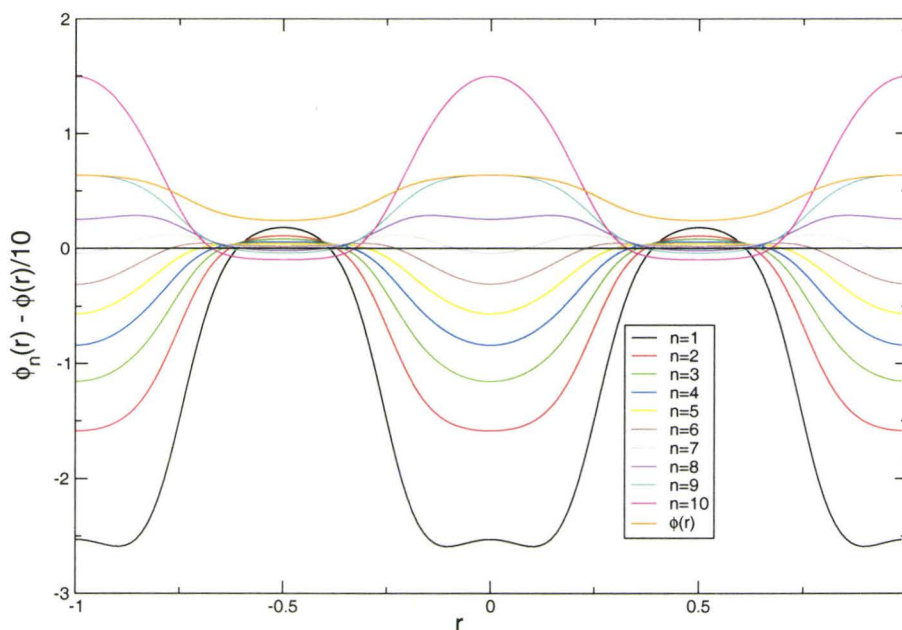


Figure 5.7: The decile composition of the hex phase at $\chi N = 13.5$, $f = 0.35$, $\kappa = 0.2$. Plotted is $\phi_n(r) - \phi(r)/10$, where $\phi_n(r)$ is the volume fraction due to the n th decile of the block length distribution. For instance, $\phi_1(r)$ is density of the shortest 10% of the molecules, and $\phi_{10}(r)$ is the density of the longest 10%.

The increase in period can be seen to be due to the existence of longer blocks than in the monodisperse case. One thing to observe is that most of the interior of a phase (whether it be lamellae, cylinders, spheres, or gyroids) is at an almost

constant density of the majority component of that structures (this is actually the assumption in the strong segregation limit, where it is assumed that the interfaces of these structures are sharp, and the density inside of them constant). If this constant density is to be maintained in the monodisperse melt, some blocks are going to have to stretch out to the centre (which is entropically unfavourable), and some are going to have to curl in on themselves at the edges. However, if there are long and short blocks available, the short blocks will preferentially occupy the edges with little stretching, and the long blocks will fill up the rest, again, with little stretching. The period of the structure will change to be consistent with the length of the long blocks, as opposed to the average block length.

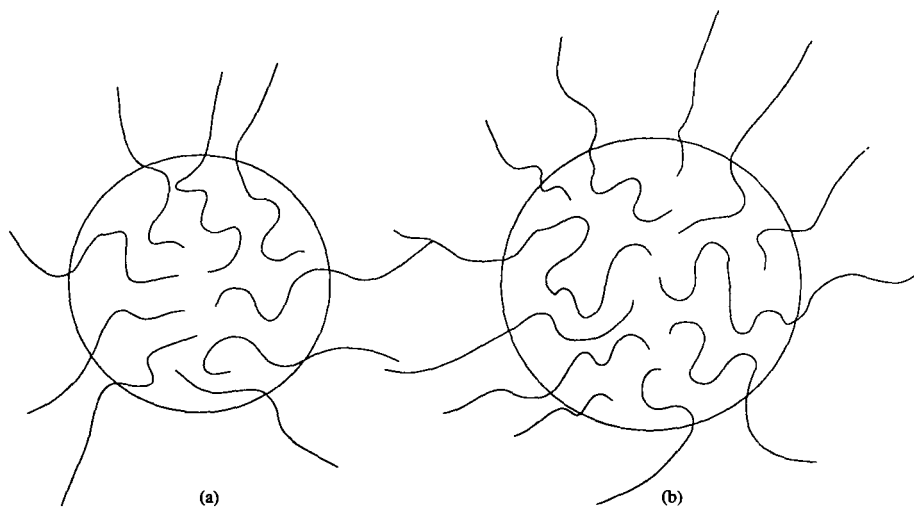


Figure 5.8: Illustration of the packing of monodisperse (a) vs. polydisperse (b) polymers in a micelle. Some polymers in (a) have to stretch to maintain a uniform density, while those in (b) can maintain more natural coils as short and long polymers fill up different areas.

5.3 Scaling

The phase diagrams in Figure 5.3 are remarkable similar. By scaling χN such that the critical points all lie on top of each other we get Figure 5.9. This scaling is approximately $\chi\tilde{N} = \chi N(1 + 0.833\kappa)$. The order-disorder transitions are seen to differ only by this scaling parameter, while the other transition lines move in.

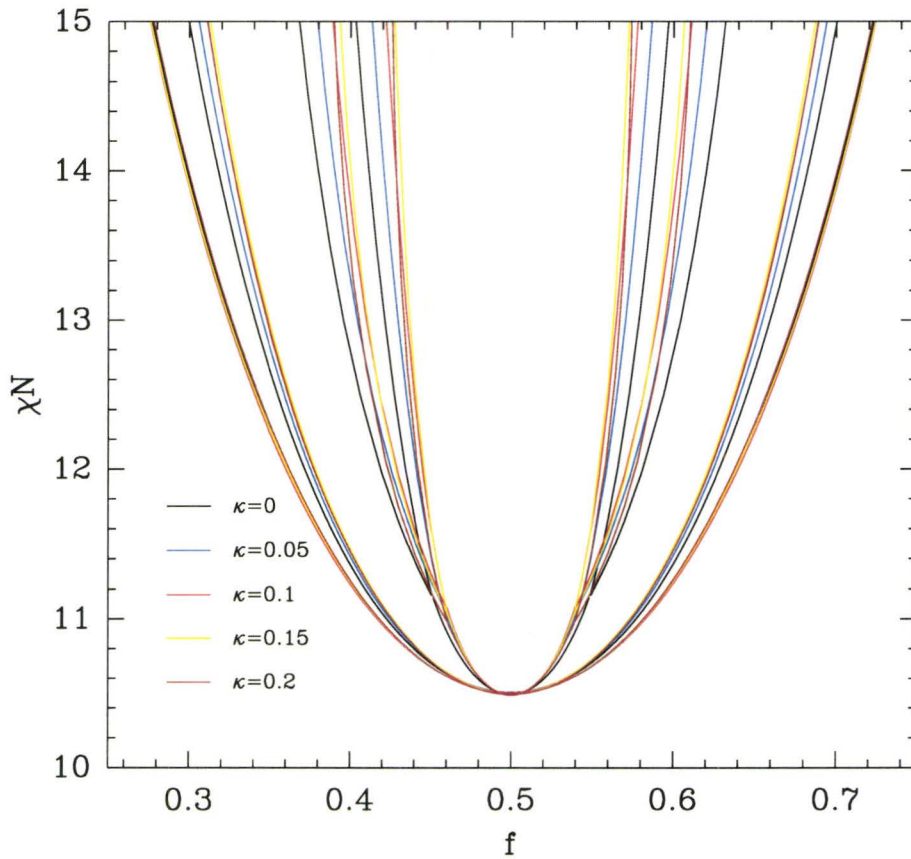


Figure 5.9: The phase diagrams for the symmetric polydisperse melts, scaled such that their critical points lie on top of each other. The values for κ run from 0 to 0.2, the larger values corresponding to the lines close to the centre.

This again suggests that the longer polymer blocks determine where the phase separation lies. By using an effective average block length $\tilde{N} = (1 + 0.833\kappa)N$,

the order-disorder transitions for polydisperse melts can be predicted from the monodisperse melt. However, the order-order transition lines do not follow this simple scaling, reflecting the fact that these transitions are driven by a delicate balance between the energy and entropy of the polymer chains.

Chapter 6

Summary

It's a poor sort of memory that only works backwards.

Lewis Carroll

Comparison of results from the random-phase approximation and from the self-consistent field theory show that the perturbation approximation to the polydispersity distribution is reasonable for small ($\kappa \lesssim 0.2$) polydispersities. While for small polydispersities the Schultz-Zimm distribution is still quite broad (Figure 2.1), using only the second moment in a perturbation approximation gives quite accurate results.

The primary effect of polydispersity (at least from an experimental perspective) would be the increase in the period of the structures formed, due to the existence of longer chains in the melt. This effect can be understood by the distribution of the chain lengths in the melt: the longer polymer blocks are denser in the middle of a microstructure than shorter blocks. For symmetric cases ($\kappa_A = \kappa_B$), the phase diagrams for the polydisperse melts are remarkable similar to that for monodisperse melts if an effective average polymer length that is larger than the actual average polymer length is used.

Another effect of polydispersity is the stabilization of non-lamellar phases. This effect can be understood by considering the packing of polymers into cylinders or

spheres. In order to maintain a constant density, polymers have to be stretched or compressed. This packing frustration can be relieved in a polydisperse system.

Experimentally observed phase diagrams are almost always asymmetric with respect to $f_A \leftrightarrow 1 - f_A$. This asymmetry is usually attributed to the asymmetry in the Kuhn length. Our study points out that polydispersity can lead to asymmetric phase diagrams also. It is desirable to design a systematic experimental test of the theory.

Extensions of this work would be to use the (non-perturbative) Schultz-Zimm distribution in SCFT (most likely requiring the evaluation of the integrals of q_α to be done numerically). In addition, including fluctuations as has been done by Shi and coworkers for the monodisperse melt [Shi99, LSND97, SND96] would give insight into how polydispersity affects the stability of the phases.

While macrophase separation was touched upon in the discussion of the RPA, it may be that phase coexistence is possible for two or more slightly different microstructures, say of two lamellar structures of different periodicities. Recent techniques due to Sollich and others [SWC01] have interesting applications to this study.

Appendix A

The Gamma Symbol

There is no other royal path which leads to geometry.

Euclid to Ptolemy I

A transform of a function $f(\mathbf{r})$ to $\tilde{f}(\mathbf{k})$ can be defined using general basis functions $\psi(\mathbf{k}; \mathbf{r})$, with the properties

$$\int d\mathbf{r} \psi^*(\mathbf{k}; \mathbf{r}) \psi(\mathbf{k}'; \mathbf{r}) = \delta(\mathbf{k} - \mathbf{k}') \quad \int d\mathbf{k} \psi^*(\mathbf{k}; \mathbf{r}) \psi(\mathbf{k}; \mathbf{r}') = \delta(\mathbf{r} - \mathbf{r}') \quad (\text{A.1})$$

$$\tilde{f}(\mathbf{k}) = \int d\mathbf{r} f(\mathbf{r}) \psi(\mathbf{k}; \mathbf{r}) \quad f(\mathbf{r}) = \int d\mathbf{k} \tilde{f}(\mathbf{k}) \psi^*(\mathbf{k}; \mathbf{r}). \quad (\text{A.2})$$

When the basis functions are the usual functions for a Fourier expansion ($\psi(\mathbf{k}; \mathbf{r}) = e^{-i\mathbf{k}\cdot\mathbf{r}}$), the convolution theorem

$$\tilde{h}(\mathbf{k}) = \int d\mathbf{q} \tilde{f}(\mathbf{q}) \tilde{g}(\mathbf{k} - \mathbf{q}) \quad (\text{A.3})$$

where $\tilde{h}(\mathbf{k})$ is the Fourier transform of $f(\mathbf{r})g(\mathbf{r})$, holds. However, for a general basis expansion, this is no longer true. Instead, a generalisation must be used:

$$\tilde{h}(\mathbf{k}) = \int d\mathbf{q} \int d\mathbf{q}' \tilde{f}(\mathbf{q}) \tilde{g}(\mathbf{q}') \Gamma(\mathbf{q}, \mathbf{q}', \mathbf{k}) \quad (\text{A.4})$$

where the Γ symbol (introduced in Chapter 4) is

$$\Gamma(q, q', k) = \int d\mathbf{r} \psi^*(q; \mathbf{r}) \psi^*(q'; \mathbf{r}) \psi(k; \mathbf{r}). \quad (\text{A.5})$$

Note that for the Fourier basis functions, $\Gamma(q, q', k) = \delta(q + q' - k)$. The Γ symbol is required for finding the basis function expansion of the product of two functions from the expansions of the functions. However, calculating its value is complicated and (human) error-prone. The purpose of this appendix is to show an efficient method for calculating it for the special case where the basis functions have the symmetry of a space group.

A.1 Structure of a space group¹

An infinite space group is a group G which maps an infinite lattice \mathcal{L} into itself. A lattice vector $\mathbf{r}_n \in \mathcal{L}$ is represented as

$$\mathbf{r}_n = n_1 \mathbf{a}_1 + n_2 \mathbf{a}_2 + n_3 \mathbf{a}_3, \quad (\text{A.6})$$

where $n_1, n_2, n_3 \in \mathbb{Z}$, and $\mathbf{a}_1, \mathbf{a}_2, \mathbf{a}_3$ are three non-coplanar vectors forming the basis. The elements of G are those elements S of the Euclidean group E_3 such that $\mathbf{r}'_n = S\mathbf{r}_n$ where $\mathbf{r}'_n \in \mathcal{L}$. All elements of E_3 can be thought of as a rotation (including improper rotations) followed by a translation. The rotation can be represented by a matrix α in $O(3)$, and the translation is a vector $\mathbf{t} \in \mathbb{R}^3$. An element of E_3 will be written as $S = (\alpha, \mathbf{t})$. The operation of S on \mathbf{r} is then $S\mathbf{r} = \alpha\mathbf{r} + \mathbf{t}$.

A few useful properties (where $S_1 = (\alpha_1, \mathbf{t}_1)$ and $S_2 = (\alpha_2, \mathbf{t}_2)$) are

$$S_2 S_1 = (\alpha_2 \alpha_1, \alpha_2 \mathbf{t}_1 + \mathbf{t}_2) \quad (\text{A.7})$$

¹Most of this section was derived from [Cra68] and [Mar62].

$$S^n = (\alpha^n, (\alpha^{n-1} + \alpha^{n-2} + \cdots + 1)t) \quad (\text{A.8})$$

$$S^{-1} = (\alpha^{-1}, -\alpha^{-1}t) \quad (\text{A.9})$$

We will first consider the constraints on pure translations (I, t) . We have

$$\mathbf{r}'_n = (I, t)\mathbf{r}_n = \mathbf{r}_n + t. \quad (\text{A.10})$$

Since \mathbf{r}'_n and \mathbf{r}_n are both in \mathcal{L} , t must also. The subgroup of G composed of translations (I, \mathbf{r}_n) is the subgroup T of primitive translations of G . It is an invariant subgroup as $T = G^{-1}TG$.

It can be shown that the matrices α are rotations whose rotation axes lie along one of the basis vectors, and the rotation angle is $2\pi m/n$, where $m \in \mathbb{Z}$ and $n = 1, 2, 3, 4, 6$. Thus, there always exists an integer m such that $\alpha^m = 1$. Then, for an element $S = (\alpha, t) \in G$, $S^m = (\alpha^m, (\alpha^{m-1} + \alpha^{m-2} + \cdots + I)t) = (I, \{\alpha\}t)$ where $\{\alpha\} = \alpha^{m-1} + \alpha^{m-2} + \cdots + I$. S^m must then be a primitive translation. Let $t = v_\alpha + \mathbf{r}_n$ where $\mathbf{r}_n \in \mathcal{L}$ and v_α is a non-primitive translation

$$v_\alpha = v_1 \mathbf{a}_1 + v_2 \mathbf{a}_2 + v_3 \mathbf{a}_3 \quad v_i \in [0, 1). \quad (\text{A.11})$$

$\{\alpha\}v_\alpha$ must then be a primitive translation since $\{\alpha\}t$ is. The implication of this is that every $S \in G$ can be represented as a product of an element with a non-primitive translation and element which is just a primitive translation. The set of symmetry elements (α, v_α) with non-primitive translations form a subgroup \mathcal{G} which is the factor group G/T .

The point group G_p of G is composed of the elements $(\alpha, 0)$ and is isomorphic to \mathcal{G} . There are 32 point groups. When the point group is identical to the factor group, the space group is called symmomorphic, and there are 73 of these. The other 157 are nonsymmomorphic, and are characterised by having screw axes and

glide planes.

Basis vectors \mathbf{b}_i for the reciprocal lattice are defined by the condition

$$\mathbf{a}_i \cdot \mathbf{b}_j = 2\pi\delta_{ij} \quad (i, j = 1, 2, 3) \quad (\text{A.12})$$

Then the reciprocal lattice \mathcal{L}^{-1} is composed of vectors

$$\mathbf{k}_n = k_1\mathbf{b}_1 + k_2\mathbf{b}_2 + k_3\mathbf{b}_3 \quad (\text{A.13})$$

where $k_i \in \mathbb{Z}$. The important property is $e^{i\mathbf{k}_m \cdot \mathbf{r}_n} = 1$ if $\mathbf{k}_m \in \mathcal{L}^{-1}$ and $\mathbf{r}_n \in \mathcal{L}$.

A.2 Basis functions

For solving the modified diffusion equation, we wish to expand functions of \mathbf{r} in terms of basis functions which have the symmetry of \mathcal{G} . These are

$$f_{\mathbf{k}}(\mathbf{r}) = \sum_{S \in \mathcal{G}} e^{i\mathbf{k} \cdot S^{-1}\mathbf{r}} \quad (\text{A.14})$$

where the functions are indexed by reciprocal space vectors \mathbf{k} .

Let P_L be the operator on the space of functions associated with element L of G , such that

$$P_L f(\mathbf{r}) = f(L^{-1}\mathbf{r}). \quad (\text{A.15})$$

A little thought shows that the operators P_L form a group which is isomorphic to the group G . For f to have the symmetry of the space group it must first be invariant under primitive translations. Let L be the primitive translation (I, \mathbf{r}_n) . Then $P_L f_{\mathbf{k}}(\mathbf{r})$ is

$$f_{\mathbf{k}}(L^{-1}\mathbf{r}) = f_{\mathbf{k}}(\mathbf{r} - \mathbf{r}_n) \quad (\text{A.16})$$

$$= \sum_{S \in \mathcal{G}} e^{ik \cdot S^{-1}(r-r_n)} \quad (\text{A.17})$$

$$= \sum_{S \in \mathcal{G}} e^{ik \cdot S^{-1}r} e^{-ik \cdot r_n}. \quad (\text{A.18})$$

Since L is a primitive translation of the real-space lattice, $k \cdot r_n$ will be an integer multiple of 2π , so $P_L f_k(r) = f_k(r)$.

Knowing that f is invariant under primitive translations, it is enough to show that it also invariant under $L \in \mathcal{G}$ since any element of G can be decomposed as a product of a primitive translation and an element of \mathcal{G} . Letting $L \in \mathcal{G}$,

$$f_k(L^{-1}r) = \sum_{S \in \mathcal{G}} e^{ik \cdot S^{-1}L^{-1}r} \quad (\text{A.19})$$

$$= \sum_{S \in \mathcal{G}} e^{ik \cdot (LS)^{-1}r}. \quad (\text{A.20})$$

Since LS will run over all elements of \mathcal{G} just as S does, the last sum is equivalent to (A.14).

As given, the $f_k(r)$ are not orthogonal. Choosing a representative vector $g_n \in \mathcal{L}^{-1}$, all reciprocal space vectors $k = \alpha g_n$ with $(\alpha, 0) \in G_p$ will have $f_k(r)$ equal to within a constant multiplicative factor. The set

$$K_n^* = G_p g_n = \{ \alpha g_n \mid (\alpha, 0) \in G_p \} \quad (\text{A.21})$$

is the orbit of g_n under the group action of the point group G_p .² A reciprocal-space vector can then be classified by an index n of the orbit K_n^* it belongs to. The orbits will be ordered by the length of the vectors in the orbit. Let $N_n = |K_n^*|$ be the number

²The term "orbit" here is from mathematics. The term "star" has been used in physics to denote this collection of reciprocal lattice vectors. Since this appendix is an attempt at mathematical rigour, the more general "orbit" will be used instead of "star".

of vectors in the n th orbit. Using $S = (\alpha, v_\alpha)$ in (A.14) gives

$$f_n(\mathbf{r}) = \sum_{(\alpha, v_\alpha) \in G_p} e^{i\mathbf{g}_n \cdot (\alpha^{-1}, -\alpha^{-1}v_\alpha)\mathbf{r}} \quad (\text{A.22})$$

$$= \sum_{(\alpha, v_\alpha) \in G_p} e^{i(\alpha\mathbf{g}_n)\mathbf{r}} e^{i\mathbf{g}_n \cdot (-\alpha^{-1}v_\alpha)} \quad (\text{A.23})$$

where we have used the property that $\mathbf{a} \cdot (\alpha\mathbf{b}) = (\alpha^{-1}\mathbf{a}) \cdot \mathbf{b}$ when α is orthogonal. For convenience, let $\mathbf{p}_\alpha = -\alpha^{-1}v_\alpha$. It can be seen then that the sum has only N_n unique components, corresponding to the elements of the orbit of \mathbf{g}_n . The basis functions can then be rewritten as

$$f_n(\mathbf{r}) = \frac{1}{\sqrt{N_n}} \sum_{k_i \in K_n^*} e^{ik_i \cdot \mathbf{r}} S_i^n \quad (\text{A.24})$$

where $1/\sqrt{N_n}$ is a normalising factor, and

$$S_i^n = \sum_{\substack{(\alpha, v_\alpha) \in \mathcal{G} \\ \alpha k_i = k_i}} e^{-ik_i \cdot \alpha v_\alpha} \quad (\text{A.25})$$

is a phase factor. For a cubic phase, in general $S_i^n = \pm 1$, but this is not necessarily true for non-cubic phases. Systematic absences may also occur where the individual phase factors in (A.25) cancel each other out.

A function $g(\mathbf{r})$ can then be expanded as

$$g(\mathbf{r}) = \sum_n g_n f_n(\mathbf{r}) \quad (\text{A.26})$$

where g_n is found by multiplying both sides by $f_m(\mathbf{r})$ and integrating.

Two functions multiplied together gives

$$g(\mathbf{r})h(\mathbf{r}) = \sum_n \sum_m g_n h_m f_n(\mathbf{r}) f_m(\mathbf{r}). \quad (\text{A.27})$$

The coefficients of the product $c(\mathbf{r}) = g(\mathbf{r})h(\mathbf{r})$ are found by multiplying by $f_l(\mathbf{r})$ and integrating:

$$c_l = \int d\mathbf{r} g(\mathbf{r})h(\mathbf{r})f_l(\mathbf{r}) = \sum_n \sum_m g_n h_m \int d\mathbf{r} f_n(\mathbf{r})f_m(\mathbf{r})f_l(\mathbf{r}). \quad (\text{A.28})$$

Define

$$\Gamma_{nml} = \int d\mathbf{r} f_n(\mathbf{r})f_m(\mathbf{r})f_l(\mathbf{r}). \quad (\text{A.29})$$

This is our Γ symbol. It has the same relation to the coefficients of $g(\mathbf{r})h(\mathbf{r})$ as δ_{nm} has to the coefficients of $g(\mathbf{r})$. Using Γ , c_l is then

$$c_l = \sum_n \sum_m \Gamma_{nml} g_n h_m. \quad (\text{A.30})$$

Substituting (A.24) into (A.29) gives

$$\Gamma_{nml} = \frac{1}{\sqrt{N_n N_m N_l}} \sum_{\substack{k_i \in K_n^* \\ k_j \in K_m^* \\ k_k \in K_l^*}} \int d\mathbf{r} e^{i(k_i + k_j + k_k) \cdot \mathbf{r}} S_i^n S_j^m S_k^l. \quad (\text{A.31})$$

The integral evaluates to a Kronecker delta (since the integral is done over a primitive cell). Hence,

$$\Gamma_{nml} = \frac{1}{\sqrt{N_n N_m N_l}} \sum_{\substack{k_i \in K_n^* \\ k_j \in K_m^* \\ k_k \in K_l^*}} [k_n + k_m + k_l = 0] S_i^n S_j^m S_k^l. \quad (\text{A.32})$$

where $[b]$ is Iverson's convention, which is 1 if the Boolean expression b is true, and 0 otherwise. As used above, it is equivalent to a Kronecker delta, but is more extensible.

A.3 Simplification of Γ_{nml}

From now on the prefactor $1/\sqrt{N_n N_m N_l}$ will be dropped. The restriction $k_n + k_m + k_l = 0$ means Γ_{nml} can be written

$$\Gamma_{nml} = \sum_{k_i \in K_n^*} \sum_{k_j \in K_m^*} [-k_i - k_j \in K_l^*] S_i^n S_j^m S_k^l \quad (\text{A.33})$$

For simplicity, the phase factors S_i^n will be assumed to be 1 from here on. This applies to the lamellar, hex, and bcc phases³. Running over every vector in $\mathcal{G}g$ can be expanded to running over every symmetry operation O in \mathcal{G} , dividing by the multiplicity $\varepsilon_n = |\mathcal{G}|/N_n$. Using this gives

$$\varepsilon_n \varepsilon_m \Gamma_{nml} = \sum_{O_n \in \mathcal{G}} \sum_{O_m \in \mathcal{G}} [-O_n g_n - O_m g_m \in \mathcal{G}g_l] \quad (\text{A.34})$$

Now, $-O_n g_n - O_m g_m \in \mathcal{G}g_l$ iff $\exists O_l \in \mathcal{G}$ s.t. $-O_n g_n - O_m g_m = O_l g_l$. Since \mathcal{G} is a group, this statement is equivalent to $\exists O_l \in \mathcal{G}$ s.t. $-g_n - O_n^{-1} O_m g_m = O_l g_l$. But O_m also runs over all $O \in \mathcal{G}$, so $O_n^{-1} O_m$ can be replaced by O_m by changing the order of summation. This removes all O_n terms, so that sum can be pulled out and is equal to $|\mathcal{G}|$. Changing the m sum back to a sum over $\mathcal{G}g_m$ gives

$$\Gamma_{nml} = N_n \sum_{k \in \mathcal{G}g_m} [-g_n - k \in \mathcal{G}g_l]. \quad (\text{A.35})$$

Since Γ_{nml} is cyclic in its indices, it will also be a multiple of N_m and N_l . In general, it will be a multiple of the least common multiple of N_n , N_m , and N_l .

³Note that this can be extended to $S_i^n \neq 1$, however, it's more complicated.

Bibliography

- [Ang98] H.J. Angerman, *The phase behaviour of polydisperse multiblock copolymer melts (a theoretical study)*, Ph.D. thesis, Department of Polymer Chemistry and Materials Science, University of Groningen, Nijenborgh 4, 9747 AG, Groningen, January 1998.
- [AtBS99] H.J. Angerman, G. ten Brinke, and J.J.M Slot, *Influence of polydispersity on the phase behaviour of statistical multiblock copolymers with Schultz-Zimm block molecular weight distributions*, Eur. Phys. J. B **12** (1999), 397–404.
- [Bra75] S.A. Brazovskii, *Phase transition of an isotropic system to a nonuniform state*, Sov. Phys.-JETP **41** (1975), no. 1, 85–89.
- [BRS90] C. Burger, W. Ruland, and A.N. Semenov, *Polydispersity effects on the microphase-separation transition in block copolymers*, Macromolecules **23** (1990), 3339–3346.
- [Cra68] Arthur P. Cracknell, *Applied group theory*, Pergamon Press, 1968.
- [Doi97] Masao Doi, *Introduction to polymer physics*, Oxford U.P., 1997.
- [Dub] Paul Dubois, *Numerical Python* <http://www.numpy.org>.
- [Edw66] S.F. Edwards, *The theory of polymer solutions at intermediate concentration*, Proc. Phys. Soc. **88** (1966), 265–280.

- [FH87] Glenn H. Fredrickson and Eugene Helfand, *Fluctuation effects in the theory of microphase separation in block copolymers*, J. Chem. Phys. **87** (1987), no. 1, 697–705.
- [Flo49] P.J. Flory, *The conformation of real polymer chains*, J. Chem. Phys. **17** (1949), 303.
- [Hah99] Theo Hahn (ed.), *International tables for crystallography*, second ed., vol. A, Kluwer Academic Publishers, 1999.
- [Hel75] Eugene Helfand, *Theory of inhomogeneous polymers: Fundamentals of the Gaussian random-walk model*, J. Chem. Phys. **62** (1975), no. 3, 999–1005.
- [Hie84] Paul C. Hiemenz, *Polymer chemistry*, Marcel Dekker, Inc., 1984.
- [HN84] K.M. Hong and Jaan Noolandi, *The effect of polydispersity on the microphase separation of a block copolymer system*, Polymer Comm. **25** (1984), no. 9, 265.
- [HS82] George Hadziioannou and Antoine Skoulios, *Structural study of mixtures of styrene/isoprene two- and three-block copolymers*, Macromolecules **15** (1982), 267–271.
- [HSK80] Takeji Hashimoto, Mitsuhiro Shibayama, and Hiromichi Kawai, *Domain-boundary structure of styrene-isoprene block copolymer films cast from solution. 4. molecular-weight dependence of lamellar microdomains*, Macromolecules **13** (1980), 1237–1247.
- [Kro90] J.I. Kroschwitz (ed.), *Polymers: Polymer characterization and analysis*, John Wiley & Sons, 1990.
- [Lei80] Ludwik Leibler, *Theory of microphase separation in block copolymers*, Macromolecules **13** (1980), 1602–1617.

- [LSND97] Mohamed Laradji, An-Chang Shi, Jaan Noolandi, and Rashmi C. Desai, *Stability of ordered phases in diblock copolymer melts*, *Macromolecules* **30** (1997), no. 11, 3242–3255.
- [Mar62] L. Mariot, *Group theory and solid state physics*, Prentice-Hall, Inc., 1962.
- [MB96] M. W. Matsen and F.S. Bates, *Unifying weak- and strong-segregation block copolymer theories*, *Macromolecules* **29** (1996), no. 4, 1091–1098.
- [MS94] M.W. Matsen and M. Schick, *Stable and unstable phases of a diblock copolymer melt*, *Phys. Rev. Lett.* **72** (1994), no. 16, 2660–2663.
- [Ros] Guido Rossum, *Python programming language* <http://www.python.org>.
- [Sem85] A.N. Semenov, *Contribution to the theory of microphase layering in block-copolymer melts*, *Sov. Phys. JETP* **61** (1985), no. 4, 733–742.
- [Shi99] An-Chang Shi, *Nature of anisotropic fluctuation modes in ordered systems*, *J. Phys.: Condens. Matter* **11** (1999), 10183–10197.
- [SND96] An-Chang Shi, Jaan Noolandi, and Rashmi C. Desai, *Theory of anisotropic fluctuations in ordered block copolymer phases*, *Macromolecules* **29** (1996), 6487–6504.
- [Str97] Gert Strobl, *The physics of polymers*, second ed., Springer, 1997.
- [SWC01] Peter Sollich, Patrick B. Warren, and Michael E. Cates, *Moment free energies for polydisperse systems*, *Advances in Chemical Physics*, vol. 116, John Wiley & Sons, 2001, also available as arXiv:cond-mat/0003084, pp. 266–336.
- [Wie86] F.W. Wiegels, *Introduction to path-integral methods in physics and polymer science*, World Scientific, 1986.

- [WN90] M.D. Whitmore and Jaan Noolandi, *Self-consistent theory of block copolymer blends: Neutral solvent*, J. Chem. Phys. **93** (1990), no. 4, 2946–2955.
- [WV92] M.D. Whitmore and J.D. Vavasour, *Self-consistent mean field theory of the microphase diagram of block copolymer/neutral solvent blends*, Macromolecules **25** (1992), 2041–2045.
- [Zim48] B.H. Zimm, *Light scattering of polystyrene*, J. Chem. Phys. **16** (1948), 1099.